คุณสมบัติการวัดรังสีของเครื่องฉายรังสีเอกซ์พลังงานสูงชนิดอะมอฟัสซิลิกอน
เพื่อการตรวจสอบการฉายรังสีแบบปรับความเข้ม

นายณัฏฐกร ปรีดาศักดิ์

DOSIMETRIC PROPERTIES OF AMORPHOUS SILICON ELECTRONIC PORTAL IMAGING DEVICE FOR VERIFICATION OF DYNAMIC INTENSITY MODULATED RADIATION THERAPY

Mr. Nuttakorn Preedasak

Thesis Title   Dosimetric properties of amorphous silicon electronic portal imaging device for verification of dynamic intensity modulated radiation therapy

By   Mr. Nuttakorn Preedasak

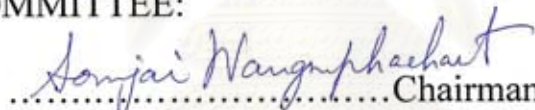Field of study   Medical Imaging

Thesis Advisor   Associate Professor Sivalee Suriyapee, M.Eng.

Thesis Co-advisor   Miss. Chulee Charoonsantikul, M.Sc.

Accepted by the Faculty of Medicine, Chulalongkorn University in Partial Fulfillment of the Requirements for the Master's Degree

.........Dean of the Faculty of Medicine
(Professor Pirom Kamol-ratanakul, M.D., M.Sc.)

THESIS COMMITTEE:

..............Chairman
(Associate Professor Somjai Wangsuphachart, M.D.)

....Thesis Advisor
(Associate Professor Sivalee Suriyapee, M.Eng.)

.........Thesis Co-advisor
(Miss. Chulee Charoonsantikul, M.Sc.)

.........Member
(Associate Professor Anchali Krisanachinda, Ph.D.)

.........Member
(Mrs. Weeranuch Kitsukjit, M.Sc.)

ณัฏฐกร ปรีดาศักดิ์ : คุณสมบัติการวัดรังสีของเครื่องฉายรังสีเอกซ์พลังงานสูงชนิดอะมอฟัสซิลิกอนเพื่อการตรวจสอบการฉายรังสีแบบปรับความเข้ม. (DOSIMETRIC PROPERTIES OF AMORPHOUS SILICON ELECTRONIC PORTAL IMAGING DEVICE FOR VERIFICATION OF DYNAMIC INTENSITY MODULATED RADIATION THERAPY). อ.ที่ปรึกษา: รศ. ศิวลี สุริยาปี, อ.ที่ปรึกษาร่วม: นางสาวชูลี จรูญสันติกุล; 75 หน้า ISBN 974-53-2581-3

วัตถุประสงค์ของงานวิจัยนี้เพื่อศึกษาคุณสมบัติพื้นฐานการวัดรังสีของเครื่องฉายภาพรังสีเอกซ์พลังงานสูง ชนิดอะมอฟัสซิลิกอน รุ่น aS500 ของบริษัท Varian เพื่อนำไปใช้ในการตรวจสอบการกระจายของปริมาณรังสีก่อนการ รักษาจริงด้วยการฉายรังสีแบบที่สามารถปรับความเข้มได้ งานวิจัยนี้ทดลองกับรังสีเอกซ์ขนาด 6 เมกะโวลต์จากเครื่องเร่ง อนุภาครุ่น 23EX ของบริษัท Varian และจะใช้โปรแกรม AM maintenance และ portal dosimetry ในการแสดง ภาพและค่าปริมาณรังสี คุณสมบัติพื้นฐานที่จะศึกษานั้นประกอบไปด้วย การตอบสนองของสัญญาณต่อขนาดลำรังสี อัตราปริมาณรังสีและปริมาณรังสี การสูญเสียของสัญญาณในระหว่างการรับสัญญาณ ความสัมพันธ์ของสัญญาณเมื่อเกิด การเปลี่ยนแปลงของอัตราปริมาณรังสีในขณะที่ฉายรังสีแบบปรับความเข้ม การค้างของสัญญาณในเครื่องฉายภาพ และ การทดลองความแม่นยำในการวัดปริมาณรังสีแบบเต็มพื้นที่สี่เหลี่ยมและแบบที่มีการใส่ตัวกรองปริมาณรังสีรูปลิ่ม ซึ่ง เปรียบเทียบกับการวัดด้วยไอออนแชมเบอร์ สุดท้ายทดลองเปรียบเทียบระหว่างค่าที่ได้จากการคำนวณกับค่าที่ได้จากการ วัดจริงในการฉายแบบปรับความเข้ม

จากการผลการทดลองที่ขนาดลำรังสีกว้าง เครื่องฉายตอบสนองดีกว่าขนาดลำรังสีแคบ ความสัมพันธ์ระหว่าง สัญญาณกับอัตราปริมาณรังสีและปริมาณรังสีเป็นเชิงเส้นตรง การสูญเสียของสัญญาณเกิดขึ้นจากการโอนข้อมูลซึ่งเริ่มเกิด ที่ปริมาณรังสีเท่ากับ 40 MU ทุกขนาดลำรังสีที่ทดลองซึ่งได้แก่ 4 x 4, 10 x 10 และ 15 x 15 ซม^2 และมีค่าความ ผิดพลาดถึง 17.62% ในส่วนที่มีการฉายแบบปรับความเข้มที่มีอัตราความเร็วเท่ากับ 1 เซนติเมตรต่อวินาที การ เปลี่ยนแปลงของอัตราปริมาณรังสีในขณะที่ฉายรังสีแบบปรับความเข้มไม่มีผลกระทบต่อการรับสัญญาณ การค้างของ สัญญาณในเครื่องจะน้อยลงถ้าช่วงเวลาในการฉายมากกว่า 15 วินาที ในการเปรียบเทียบกับการวัดด้วยไอออนแชมเบอร์ ในลำรังสีแบบเปิดเต็มพื้นที่โปรไฟล์ที่ได้มีลักษณะใกล้เคียงกัน ในขนาดลำรังสีกว้างและจะมากว่าเล็กน้อยในขนาดลำ รังสีแคบ ส่วนการฉายแบบใส่ตัวกรองปริมาณรังสีรูปลิ่ม จะมีค่าใกล้เคียงกันในช่วงตรงกลางและคลาดเคลื่อนเล็กน้อย ในช่วงขอบของลำรังสี สุดท้ายผลการเปรียบเทียบระหว่างค่าปริมาณการกระจายของรังสีในการรักษาด้วยรังสีแบบปรับ ความเข้มในผู้ป่วยที่เป็นมะเร็งโพรงจมูก พบว่าค่าที่เครื่องคำนวณกับที่เครื่องวัดได้มีค่าความคลาดเคลื่อนที่ได้อยู่ภายใน 3 มิลลิเมตรและความแตกต่างของปริมาณรังสีไม่เกิน 3%

งานวิจัยแสดงให้เห็นว่าถ้าเข้าใจถึงความสัมพันธ์ระหว่างค่าพิกเซลที่ได้จากเครื่องฉายภาพกับปริมาณรังสีที่ ได้รับ รวมทั้งองค์ประกอบต่างๆที่เกี่ยวข้อง ก่อนที่จะนำมาใช้ในการวัดรังสี ทำให้สามารถใช้เครื่องฉายภาพในการวัดรังสี ได้อย่างถูกต้อง ซึ่งจากผลการทดลองเครื่องฉายภาพรังสีชนิดอะมอฟัสซิลิกอนสามารถที่จะนำมาใช้ในการตรวจสอบการ ประจายของปริมาณรังสีก่อนการฉายแบบปรับความเข้มได้อย่างถูกต้องแม่นยำ สะดวก และ ประหยัดเวลา

ภาควิชา	รังสีวิทยา	ลายมือชื่อนิสิต	ณัฏฐกร ปรีดาศักดิ์
สาขาวิชา	ฉายาเวชศาสตร์	ลายมือชื่ออาจารย์ที่ปรึกษา	ศิวลี สุริยาปี
ปีการศึกษา	2548	ลายมือชื่ออาจารย์ที่ปรึกษาร่วม	ชูลี จรูญสันติกุล

4774720130: MAJOR MEDICAL IMAGING

The purpose of this study is to investigate the basic dosimetric characteristics of flat panel amorphous silicon (a-Si) detectors (aS500, Varian medical systems) for the possibility of using a-Si portal imager for absolute dosimetric verification of the delivery of dynamic intensity modulated radiation treatment (IMRT) fields. The measurements were performed with 6 MV X-ray beams from Varian Clinac 23EX. The electronic poral imaging device (EPID) was performed in AM maintenance program and portal dosimetry mode. The studies include field size dependence, dose rate and dose response, effect of dead time in frames acquisition, dose rate fluctuations, memory effect, relative and absolute dosimetry. The portal dose image was tested by comparing the EPID profiles with the ion chamber both for open and wedge fields. The portal dose image calculated by EPID portal dosimetry was compared with the EPID measurement for clinical IMRT fields.

The results showed field size dependence of EPID, which was more sensitive than ion-chamber for larger field size but less than ion chamber in smaller field size. The EPID was linear with dose rate and integral dose. The effect of dead time in frame acquisition due to transfer to the CPU was found to start at 40 MU of field size studied which were 4 x 4, 10 x 10 and 15 x 15 cm^2. The dead time resulted in dynamic field caused error that increased with leaf speed and about 17.62% for a 1 cm leaf gap moving at 1 cm/s. The response of dose rate fluctuation at 50 and 500 MU were not different. The ghost effect was negligible by increasing the period more than 15 s between exposures. The comparison of profiles from EPID and ion chamber measurement showed the agreement for larger field size but slightly higher dose of EPID in the centre of the beam for 4 x 4 cm^2. For wedge field, both of EPID and ion-chamber profiles showed the agreement in the center part but slightly shift in the penumbra region. The larger wedge angle gave more shift than small wedge angle. The pre-treatment verification for two fields of IMRT showed the agreement of absolute dose distribution between EPID calculation and EPID measurement within 3% difference in dose and 3 mm. difference in distance. The profile in the direction of MLC movement showed good correlation between calculation and measurement.

The research has demonstrated that an understanding of the relationship between pixel value reading and dose or fluence is a prerequisite for portal dosimetry. The EPID is suitable to be used for the IMRT pre-treatment verification.

Department	Radiology	Student's signature _Nuttakorn Preedasak_
Field of study	Medical imaging	Advisor's signature _Sivalee Suriyapee_
Academic	2548	Co-advisor's signture _Chulee Charoonsantikul_

ACKNOWLEDGEMENTS

CONTENTS

CONTENTS

CONTENTS

CONTENTS

CHAPTER **Page**

LIST OF TABLES

LIST OF FIGURES

Figure		Page

LIST OF FIGURES

LIST OF FIGURES

Figure   **Page**

LIST OF FIGURES

Figure   **Page**

LIST OF ABBREVIATIONS

Abbreviation	Terms
3-DCRT	Three dimensional conformal radiation therapy
A/D	Analog to digital
ACPU	Acquisition center process unit
a-Si, aSi	Amorphous silicon
BEV	Beam's eye view
C	Culomb
CT	Computed Tomography
CU	Calibrated unit
CCD	Charged coupled device
CPU	Center process unit
CSF	Collimator scatter factor
CsI	Cesium iodide
cGy	Centigray
cc	Milliliter
cm	Centimeter
cm^2	Square centimeter
cm^3	Cubic centimeter
DF	Dark field image
DMLC	Dynamic multileaf collimator
DVHs	Dose volume histrograms
d_{max}	Depth of dose maximum

LIST OF ABBREVIATIONS

Abbreviation	Terms
EPID	Electronic portal imaging device
F	Number of frames
F_c	Number of calculattion frames without dead time
F_d	Number of frames with dead time reading
FF	Flood field image
Gy	Gray
Gd_2O_2S	Gadolinium oxide sulfide
g	Gram
IDU	Image acquisition unit
ITP	Inverse treatment planning
IAS2	Image detection unit
IMRT	Intensity modulated radiation therapy
MR	Magnetic resonance
MU	Monitor unit
MV	Megavoltage
MLC	Multileaf collimator
MRI	Magnetic resonance imaging
MSF	Multiple static field
m^2	Square meter
mg	Milligram
mm	Millimeter

LIST OF ABBREVIATIONS

Abbreviation	Terms
ms	Millisecond
mm^2	Square millimeter
min	Minute
OF$_{x,y}$	Output factor
OAR	Off axis ratio
P	Pixel value
PD	Portal dose
PV	Portalvision
PDI	Portal dose image
PET	Positron emission tomography
QA	Quality assurance
R^2	R-squared value
RF$_{pi}$	Detector response function
SDD	Source detector distance
SMLC	Static multileaf collimator
s	Second
T	Acquisition time reading
TFT	Thin film transitor
TLD	Themoluminescent dosimetry
TPS	Treatment planning system
V	Voltage

CHAPTER I

INTRODUCTION

A major theme for improving of radiotherapy is dose conformation, the matching of the high-dose irradiated volume to the target volume as closely as possible while avoiding normal tissues. Accuracy in patient positioning is a prerequisite to ensure precise coverage of the tumor volume, but may well be one of the weakest links in the chain of events leading to the delivery of radiation for the treatment of cancer. Verification of the proper delivered dose in terms of field shape and localization with respect to patient anatomy is necessary to assure the safety and quality of complex radiation therapy treatments such as intensity-modulated radiotherapy (IMRT). IMRT means Intensity Modulated Radiation Therapy. This technique is used to match the target volume by modifying the fluence of several beams. A very simple example of IMRT is the use of wedges (hard wedges or virtual wedges) to modify the fluence of the beam in one direction. A precise definition of IMRT does not exist. The term is usually used for treatments with multiple fixed beams (i.e. 5 - 7 gantry angles), where each beam is divided into several subfields. The subfields are usually created by means of multileaf collimator (MLC), and for each subfield the dose rate and/or energy may be different. The subfields may be created by continuously moving the leave of the MLC (dynamic method), or by positioning the leaves with the beam switched off and keeping the leaf positions during the radiation constant (step and shoot method). Due to its complexity, IMRT presents a challenge to verify that the desired fluence and hence dose distribution is delivered by the linear accelerator. The most widely used form of pre-treatment quality assurance (QA) for IMRT verification generally consists of absolute dose measurements (with ionization chamber, diode, TLD, etc.) combined with isodose distribution measurements in a phantom (film), or even by means of gel dosimetry[1]. The actual data acquisition as well as the data handling for comparison remains a time consuming task.

A more efficient tool for IMRT pre-treatment QA is the electronic portal imaging device (EPID). EPID was originally designed and developed to replace radiographic films for purpose of geometric verification of patient set-up during treatment. This film is time consuming involving recalculation of the IMRT plan, set-up time on the linear accelerator, film calibration, film processing, digitization and comparison to the plan. The new current generation of EPID is based on semiconductor materials, namely, amorphous silicon photodiodes[2]. This device is mounted on the linac, providing real-time and digital feedback to the user. EPID showed high quality image than previous devices. Until recently EPID is possible to use as a dosimetry[3]. Multiple verification images can also be rapidly acquired without to re-enter the treatment room to adjust the new position measurement. For pre-treatment verification, the EPID image can be compared to a predicted portal dose image (PDI) calculated from the fluence map for the field. Before using EPID as a dosimetry, the relationship between EPID response and dose delivery parameters, such as dose and dose rate should be understood.

In this study the dosimetric properties of amorphous silicon EPID for verification of dynamic IMRT pre-treatment QA are investigated. These properties

include EPID calibration, field size dependence, dose rate and dose response, effect of dead time related to leaf speed in frames acquisition in dynamic field, dose-rate fluctuations, memory effect, relative and absolute dosimetry. The dose profiles measured by EPID are compared with the dose profiles measured by ion-chamber in water phantom. Finally, the portal dosimetry software is used to measure the clinical IMRT fields. All investigations in this study are used at the dose rate of 300 MU/min. Each individual frame is acquired in 0.111 s.

CHAPTER II

REVIEW OF RELATED LITERATURE

Many researches performed the dosimetric verification for various types of EPID. Van et al.[4] reported on the use of a liquid-filled portal imager for the dosimetric verification of leaf speed and pulse rate fluctuations which was quantified by means of DMLC plans especially designed for this measurement. The dose profiles were comparing with film and ion-chamber. Other factors influence the accuracy of the doimetry (e.g. the need for buildup). They compared dosimetric EPID images with the corresponding image prediction delivered without a patient in the beam. The dosimetric accuracy of the measured dose distribution is 2% with respect to film and ion-chamber measurements. The accuracy declines when leaf speed is increased beyond 2 cm/s, but is fairly insensitive to accelerator pulse. The memory effect is found to be of no clinical relevance. When comparing the acquired and expected distributions, an overall agreement of 3% can be obtained, except at areas of steep dose gradients where slight positional shifts are translated into large error.

A recent publication by Greer and Popescu[5] investigated the dosimetric properties of a-Si EPID using a continue frame-averaging acquisition mode and a 6 MV radiation beam. Properties studied included effect of buildup, dose linearity, field size response, sampling of rapid multileaf collimator (MLC) leaf speeds, response to dose-rate fluctuations, memory effect, and reproducibility. The dependence of response on EPID calibration and a dead time in image frame acquisition occurred every 64 frames were measured. EPID measurements were also compared to ion-chamber and film for open and wedged static fields and IMRT fields. The EPID was linear with dose and dose rate, and response to MLC leaf speeds up to 2.5 cm/s was found to be linear. A field size dependent response of up 5% relative to d_{max} ion-chamber measurement was found. Reproducibility was within 0.8% (1 standard deviation) for an IMRT delivery recorded at intervals over a period of one month. The dead time in frame acquisition resulted in error in the EPID that increased with leaf speed and were over 20% for a 1 cm leaf gap moving 1.0 cm/s. The EPID measurements were also found to depend on the input beam profile utilized for EPID flood-field calibration. The EPID shows promise as a device for verification of IMRT, the major limitation currently being due to dead-time in frame acquisition.

Van et al.[6] investigated the basic dosimetric characteristic of an aSi portal imager, using an acquisition mode especially developed for portal dose (PD) integration during delivery of a static or dynamic radiation field. The dose calculation algorithm of a commercially available treatment planning system (Cadplan, Varian Medical Systems) was modified to allow prediction of the PD image, i.e. to compare the intended fluence distribution with the fluence distribution as actually delivered to the dynamic multileaf collimator. Absolute rather than relative dose prediction was applied. The PD image prediction was compared to the corresponding acquisition for several clinical IMRT field by means of the gamma evaluation method. The acquisition mode is accurate in integrating all PD over a wide range of monitor unit, provide detector saturation is avoided. Although the dose deposition behavior in the portal image detector is not equivalent to the dose to water versus measured PD distribution were self-consistent, lending itself to quality assurance measurements.

Gamma evaluations of the predicted 3% of the local field dose in combination with a distance to agreement of 3 mm. For predicting the PD distribution in such an indirect aSi detector, McCurdy et al.[7,8] explored a two step algorithm. Although portal dosimetry for static fields is certainly of interest, the gain would be larger when applicable for dynamic IMRT, even more so when it can be used for absolute dose verification.

Winkler et al.[9] studied the dosimetric properties of an amorphous silicon EPID (Elekta IVIEWGT) with respect to three photon beam qualities: 6, 10, and 25 MV. The EPID showed an excellent temporal stability on short term as well as on long term scales. Ghosting effects increased the sensitivity of the EPID. They became more pronounced with decreasing time intervals between two exposures as well as with increasing dose. It was observed that the response characteristics of our EPID depended on dose as well as on dose rate. Doubling the dose rate increased the EPID sensitivity by 1.5%. This behavior was successfully attributed to a dose per frame effect, i.e., a nonlinear relationship between the EPID signal and the dose which was delivered to the panel between two successive readouts. The sensitivity was found to vary up to 10% in the range of 1 to 1000 monitor units. This variation was governed by two independent effects. For low doses, the EPID signal was reduced due to the linac's changing dose rate during startup. For the beam qualities which were used, the response characteristics of the EPID did not depend on energy. Differences in relative dose response curves resulted from energy dependent temporal output characteristics of the accelerator. If ghosting is prevented from affecting the results and all dose response effects are properly corrected for, the EPID signal becomes independent of dose rate, dose, and exposure time.

CHAPTER III

THEORY

3.1 Intensity Modulated Radiation Therapy (IMRT)[10]

IMRT is a state-of-the-art cancer treatment method that delivers high doses of radiation directly to cancer cells in a very targeted way, much more precisely than is possible with conventional radiotherapy. IMRT can deliver higher radiation doses directly to cancer cells while sparing more of the surrounding healthy tissue. This has important advantages in oral cancers as it allows the beams to hit their target area while missing the surrounding structures such as the salivary glands.

IMRT uses computer-generated images to plan, and then deliver tightly focused radiation beams to cancerous tumors. Clinicians use it to exquisitely "paint" the tumor with a precise radiation beam that conforms as closely as possible to the shape of the tumor (fig 3.1).
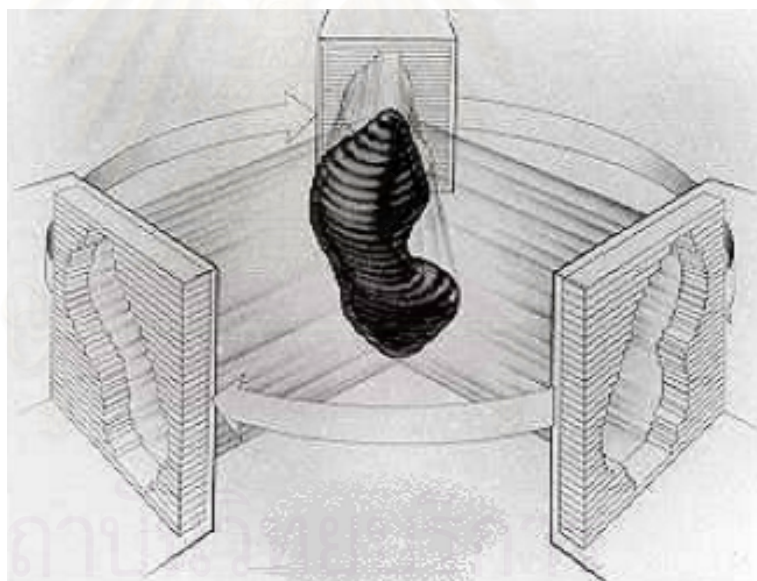
Figure 3.1 IMRT delivery

IMRT can be used to treat tumors that might have been considered untreatable in the past due to close proximity of vital organs and structures. Treating such tumors requires tremendous accuracy. The IMRT planning can be accomplished by manually adding subfields with various weights and evaluating the dose distribution. In each iteration of the process, the planner decides what changes to revise the design. The planning process is not automated and is sometimes called "forward planning" (beam parameters→dose distribution). This method typically produces a limited number of subfields and is a natural evolution of 3-D conformal planning. This method lends

itself to "step and shoot" delivery techniques. This approach can be automated to various degrees, both for designing the segments based on beam's eye view projections of targets and structures and determined the relative weight to give each segment. Another approach to IMRT planning breaks each beam into many small beamlets and determines the intensity of each. Having a large number of segments or beamlets makes the problem of determining individual intensity very complex and requires computerized intensities very complex and requires computerized methods for solution. This process has come to be called "inverse planning" (dose distribution→beam parameters). The planner specifies beam directions (or arc angles), target dose goals, and dose contains or goals for sensitive structures, and then an automated optimization algorithm calculates intensity patterns that create a dose distribution that best meets the prescription. If the planner wishes to change the result, he or she alters the objectives and re optimizes. Some systems have limited ability to modify the intensity patterns by deleting segments.

3.2 Treatment Planning[10]

Treatment planning in radiation oncology has undergone major evolution in the past several decades (fig 3.2). Early radiation treatment delivery was designed to aim at clinically visible or palpable disease. Later, radiation fields were crudely shaped with standard lead blocks around external landmarks. The introduction of the simulator in the 1960's allowed greater flexibility in beam arrangement and custom shaping of portals. The advances in simulators with fluoroscopy gained wide spread application in treatment. While clinical setups and conventional simulation are still in wide use today, CT-based treatment planning allows precise target definition and more focused (conformal) delivery of radiation dose. "Three-dimensional conformal radiation therapy" (3D-CRT) systems proliferated as a method of permitting higher dose to tumor, limiting dose to normal tissue, and ultimately improving local control and patient outcomes.

Clinical Setup and "Aim"	1900's
Multifield Arrangement based on External Landmarks and Simple Shielding	1940's
Simulation with Fluoroscopy and Beam Modification	1960's
CT-based 3D Conformal Therapy using Forward Treatment Planning	1980's
Inverse Treatment Planning and Intensity-Modulated Radiation Therapy	1994-
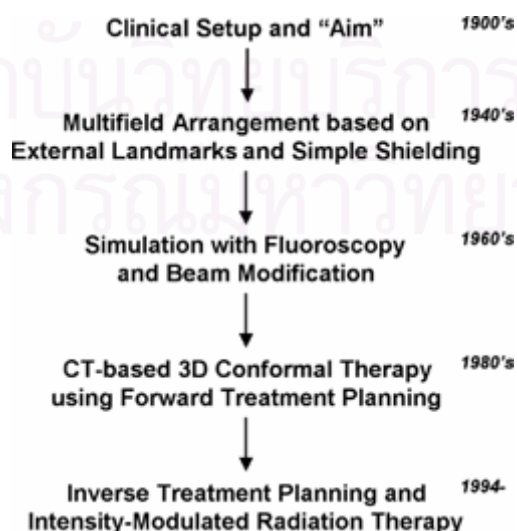
Figure 3.2 Historical perspectives in treatment planning

Treatment planning with 3D-CRT added flexibility in optimizing delivery of radiation dose to tumor while limiting normal tissue reactions. 3D-CRT allowed radiation oncologists to achieve this goal by the use of multiple portals (often 5 or 6), non-coplanar beam arrangements, proper weighting of beams, and tissue compensation for variations in tissue contour or density. Several clinical trials have demonstrated decreased normal tissue toxicity, particularly with prostate radiotherapy, and the ability to escalate dose for prostate, lung, and brain tumors. The treatment planning process also became more complex, as depicted in fig 3.3. Following patient immobilization and multiplanar imaging, traditional "forward-planning" 3D-CRT required clinicians and dosimetrists to develop beam parameters and evaluate dose distribution more or less by trial and error. For fairly routine cases such as prostate radiotherapy, various sets of standardized beam arrangements have been developed, saving themselves and others the exercise of iterative treatment planning. For more complex cases with irregular tumor contours or varying critical surrounding normal tissues, custom beam parameters need to be developed that satisfactorily deliver adequate dose to tumor while keeping surrounding doses within normal tissue tolerance. With the addition of variables such as oblique beam angles, couch rotation, and 3D dose computation, this process can often be time-consuming and sometimes may not lead to the development of an optimal plan.
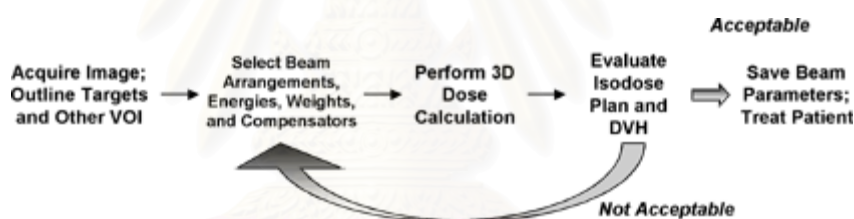
Figure 3.3 Forward 3D Treatment Planning Model

3.3 Inverse Treatment Planning[10]

In contrast to forward planning, inverse treatment planning (ITP) produces highly conformal dose distributions while minimizing the trial-and-error process. The basic planning process is outlined in fig 3.4. While the acquisition of patient data is no different, the method of generating beam parameters is revolutionized. In ITP, the radiation oncologist specifies target and normal structure volumes as well as dose restrictions on these volumes, and optimization of beam parameters is performed by computer. Although there are multiple optimization algorithms, the basic goal is to "backproject" the desired target volume isodose through the patient tissues to determine the most favorable portal geometry and radiation intensity. If the calculated isodose distribution and associated dose-volume histogram is not satisfactory, the optimization is repeated with modifications to clinical parameters, until an acceptable solution is reached. Often these iterations are used for "fine-tuning" of dose volume constraints. The mathematics of backprojection has been described over 20 years ago,

but it is now available for clinical use. Another term used is simulated annealing which is basically an inverse planning process. With the introduction of less expensive and more powerful computing equipment, this optimization process has become practical and cost-effective for many radiation oncology facilities. Automated multileaf collimation available on modern linear accelerators has allowed efficient delivery of multiple and complex portal geometries. A step-by-step outline of the planning process is further discussed below.
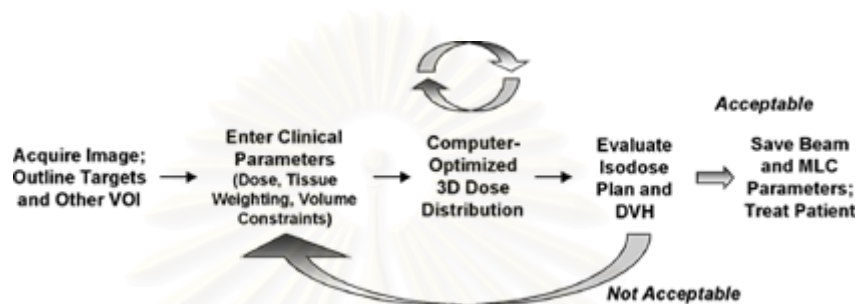
Figure 3.4 Inverse Treatment Planning Model

3.4 IMRT Treatment Planning Process[10]

Let us first briefly describe the overall process of IMRT, after which discuss the individual steps. The treatment planning steps for IMRT are similar to 3DCRT during the initial and final stages, but diverge in the middle. As shown in fig 3.5, the treatment planning process begins with treatment simulation, much the same as 3DCRT, during which the patient is set up on the CT unit in the treatment position. More and more frequently, patient CT imaging and simulation is being augmented with magnetic resonance imaging (MRI), PET, and other functional imaging studies to better define the tumor and target volume.

Simulation usually first entails fabrication of custom-designed body molds to facilitate accurate reproduction of patient position during simulation and planning, as well as during multifraction treatment delivery. After 3-D images are acquired the target and non-target structures are delineated, usually directly on a computer display of transverse CT (or MR, PET, etc.) images using standard computer graphics options such as mouse, track ball, light pen, etc.

Similarly, the design of treatment portal shapes also takes place on the computer using BEV. Using such displays one can adjust the beam directions and shapes so as to minimize the volume of normal tissues included in each radiation portal. Also superimposed on the BEV are MLC settings, such as one might design for conventional 3DCRT treatment plan. When doing an ITP, however, the treatment planner would NOT specify the MLC settings, as these would be calculated by the computer. Once all relevant tissues have been delineated, and beam directions specified, the radiation oncologist specifies the desired doses to tumor and normal

tissues. From these specifications the ITP algorithms adjust beam shapes and intensities so as to best meet these dose criteria.

IMRT incorporates (usually) computerized iteration of radiation beams as opposed to the manual optimization procedures used in conventional treatment planning. IMRT plan evaluation, as for 3 DCRT, relies largely on analysis of dose distributions and DVHs when the treatment plan has been accepted, all planning data on beam configurations and intensities are transferred to the linear accelerator (usually via a computer network, electronic chart or "record and verify" system) and patient treatment proceeds. For IMRT, the data transferred includes information on DMLC motion files required to deliver the desired X-ray intensity profiles. Finally, the physicist must perform dosimetric and QA tasks to verify that all equipment is functioning properly, and that the specifics of the dose prescription and treatment plan are accurately delivered to the patient on a daily basis.
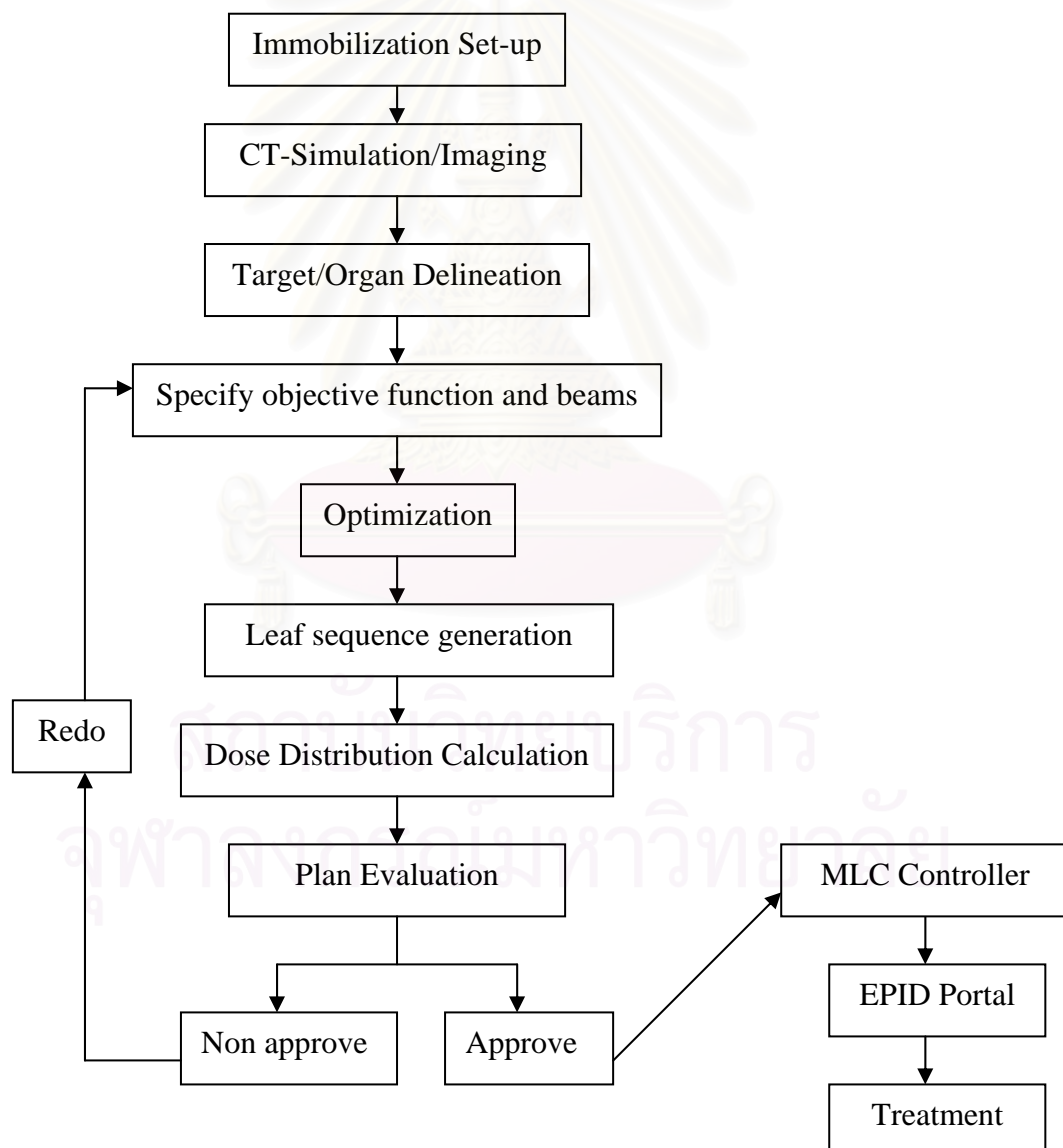
Figure 3.5 The IMRT Process

3.5 Multileaf Collimator (MLC) Moving[11]

There are two general methods of modulating a beam with a MLC. The first is based on the sequential exposure of sub-beams or segments for which the collimators are (automatically) positioned while the radiation beam is switched off. After irradiation of each segment the collimators move to the correct positions for the next segment and so on until the total modulation has been achieved. This method is known colloquially as the "step and shoot" method but is otherwise known as the multiple static field (MSF) or static MLC (SMLC) method. The use of "SMLC" has been recommended by the Intensity Modulated Radiation Therapy Collaborative Working Group in the USA and is likely to become the common term.

The second method is based on continuous irradiation during which the collimators move according to a predetermined trajectories designed to give the desired modulation. This is the dynamic MLC (DMLC) method. A comparison of the sequence of events needed to deliver a modulated beam is given in table 3.1. In each case the collimators move to a series of control points which define the position of each of the collimating elements (leaves and back up collimators) after a particular fraction of the total exposure has been delivered. There are clear similarities between both methods but it is convenient to discuss each of them separately in the following sections.

Table 3.1 The sequence of events necessary to deliver a modulated beam by the static multileaf collimator (SMLC) and the dynamic MLC (DMLC) methods

SMLC	DMLC
Move MLC to define 1st segment Irradiate with M_1 monitor units Stop irradiation Move MLC to define 2nd segment	Move MLC 1st control point Irradiate with M_1 monitor units during movement of MLC to 2nd control point
Irradiate with M_2 monitor units Stop irradiation Move MLC to define 3rd segment	Irradiate with M_2 monitor unit during movement of MLC to 3rd control point
Irradiate with M_3 monitor units Stop irradiation	Irradiate with M_3 monitor units during movement of MLC to (n+1)th control point

3.6 Dosimetric Verification of IMRT

Quality Assurance (QA) of IMRT Systematic commissioning and quality assurance are integral to the implementation of IMRT. QA of IMRT delivery systems consists of two separate issues. Machine related QA and patient related QA. Machine related QA includes leaf position accuracy, field symmetry and flatness, and dose linearity and dose accuracy; patient-specific QA includes phantom plan measurement, fluence (intensity) map check, and absolute dose verification. In general, QA of IMRT has three aspects: commissioning and testing of the treatment planning and delivery systems, routine QA of the delivery system, and patient-specific validation of treatment plans. The first aspect is concerned mainly with the integrity of the inverse planning and IMRT delivery system. The second one is concerned with the normal operation of the MLC delivery system. The third one ensures an accurate and safe treatment of a patient.

IMRT QA requires an advanced understanding of mathematical principles of dose optimization, computer-controlled delivery systems and issues that relate to the dosimetry of small and complex-shaped radiation fields. It also requires understanding of treatment setup, planning and delivery uncertainties, and their impact on patients treated with IMRT. Treatment planning optimization for IMRT is based on dose-volume constraints and dose limits for critical structures and target tissues. Therefore, understanding these concepts is also important. Overall, QA for IMRT is much more complex than QA for conventional radiation therapy.

The goal of IMRT plan validation is to verify that the correct dose and dose distribution will be delivered to the patient as calculated by the treatment planning system. To ensure proper IMRT delivery, one need to check that the plan has been computed properly and that the leaf sequence files and treatment parameters charted and/or stored in the Read/Verify system are correct and will be executable. Items that need to be validated include: monitor units (or absolute dose to a point), MLC leaf sequences or fluence maps, dose distribution, and collision avoidance. The first three items represent patient-specific IMRT QA. IMRT brings improved dose sparing of normal tissues and possibility of dose escalation, but also there is a risk to the patient from a dose error. Patient-specific QA captures the integrated results of image acquisition, segmentation, planning, agreement with the prescribed dose, and geometric and dosimetric calibration of the treatment planning and delivery systems. So in this approach, the performance of the combined system is validated and QA is aimed at identifying problems in the overall procedure. When it comes to patient-specific QA, the ideal test is to do true in vivo dosimetry and place detectors inside the patient, which does not sound like a desirable solution from the patient point of view. Instead, a patient-specific phantom study is done. In this study the IMRT plan is first generated with the patient CT scan and then patient-optimized fluences are applied to a CT scan of a water equivalent phantom. The IMRT system recalculates doses for the phantom geometry. The dosimetry verification compares the calculated and measured doses for the phantom. In implementing this process, it is assumed that if Dose measured / Dose calculated for a phantom agree within a few percent, then Dose delivered / Dose calculated in a patient should also agree within a few percent. A bonus feature of this study is that it verifies whether an accelerator

and/or MLC controls are behaving properly, at least for the day of the study. Typical techniques used for this verification are

- Film dosimetry
- Ionization chamber measurement
- Diode array measurements

To verify that the calculated dose distribution is delivered accurately during treatment, film dosimetry is usually used. In this case the IMRT plan verification procedures include phantom plan calculation (extraction of planar dose distributions), phantom and film irradiation, film developing, scanning and calibration, and finally plan/film comparison. Our question is, can a desktop computed radiography (CR) system be used for the patient-specific IMRT QA Computed radiography is a well established process for digital radiographic imaging. In comparison to film, the main CR benefits are non-chemical development of images, image quality that does not depend on processing conditions, and immediate digital storage of images. This project investigates using a CR system for patient-specific IMRT QA.

3.7 Portal Imaging[12]

Portal imaging is the use of a therapeutic X-ray beam to form an image of the area being irradiated. The historical and current main use of portal images has been the study of set-up errors in patient treatment. This has resulted in improved treatment accuracy and in quantification of the margins required to account for the uncertainties in treatment delivery. Margin quantification and reduction is an increasingly important issue for all radiotherapy departments with the increasing acceptance that conformal therapy improves patient treatment. The traditionally of portal imaging is film, called a port film (fig 3.6).
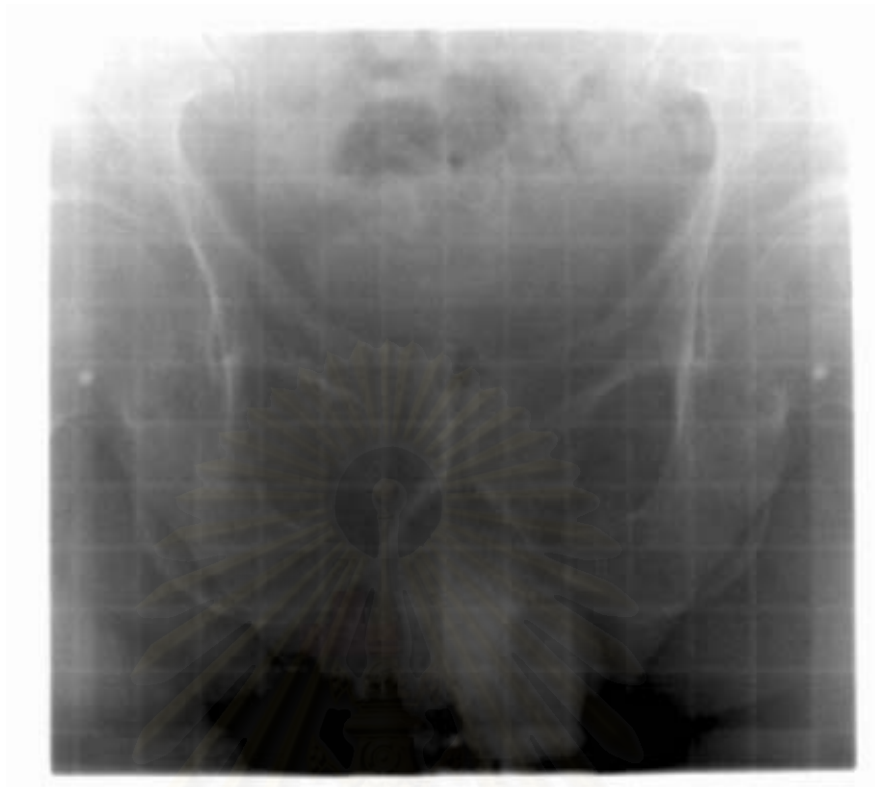
Figure 3.6 Port film

3.8 Electronic Portal Imaging Device (EPID)[12]

Electronic portal imaging device (EPID) were introduced few years ago
(fig 3.7). They were first used merely as a replacement for port films, but can also be
used to exploit the numerous advantages of digital images, in particular the possibility
of performing on-line verification (fig 3.8). However, clinical acceptance of EPID has
been limited by the poor contrast of electronic portal images, as well as an extensive
history of port film usage.

COPYRIGHT ©1999 VARIAN MEDICAL SYSTEMS

(a)

(b)

(c)

(d)

Figure 3.7 Electronic portal imaging devices (EPIDs)
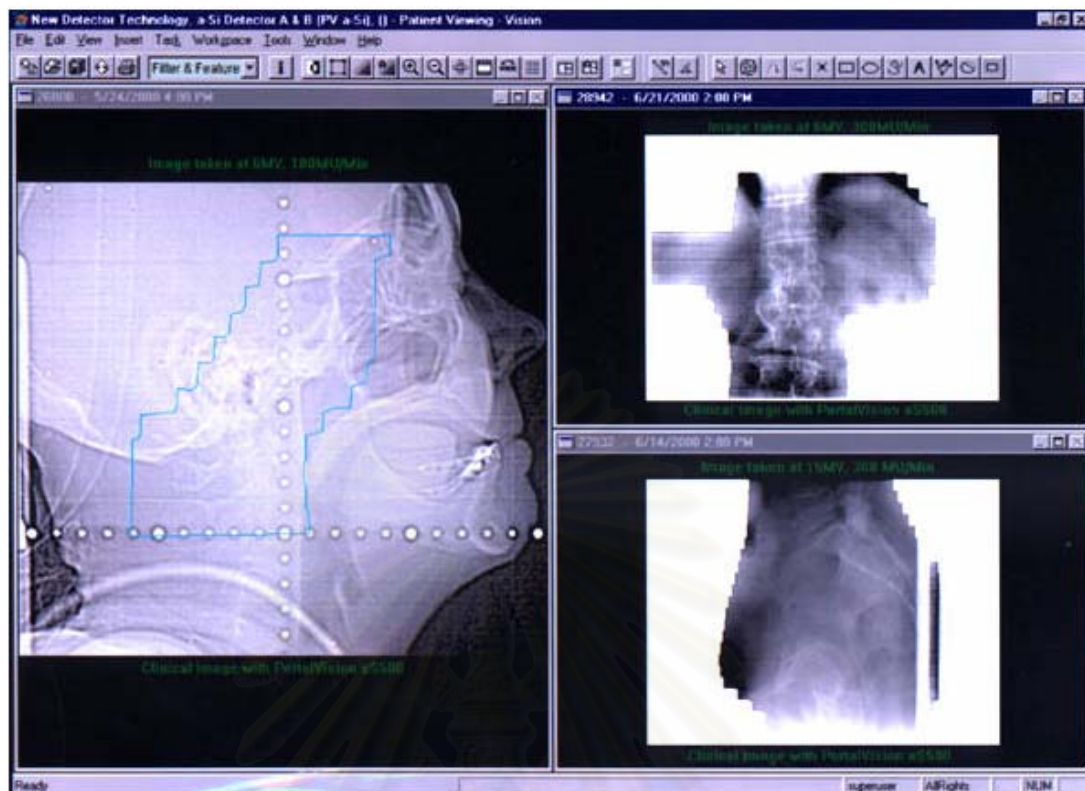
Figure 3.8 The picture from EPID for patient localization

A new generation of EPID, based on Amorphous-Silicon Flat Panel technology, is being introduced on the market. In 2000, a prototype was installed in the Department of Radiation Oncology on the dual energy Primus A LINAC. The medical community is rapidly accepting this technology as a new standard due to the high quality of images produced by this system. However, the real test of the flat panel imager is in its ability to provide useful information to the clinician.

The new flat panel has fulfilled its promises. It provides high quality portal verification images acquired with as little as 2 cGy (as compared with 7cGy for Film) of dose, while still maintaining comparable quality to our diagnostic reference films. A more efficient tool for pre-treatment QA is the electronic portal imaging device (EPID) as mounted on the linac, providing real-time, digital feedback to the user.

3.9 Technology of the Flat Panel[13]

Flat panel detector systems make use of technology similar to that used in laptop computer display, and much of this has to do with wiring the huge number of individual display elements. Instead of producing individual electrical connections to each one of the elements in a flat panel display, a series of horizontal and vertical electrical lines are used which, when combined with appropriate readout logic, can address each individual display element. With this approach only 2,000 connections between this imaging plate and the readout electronics are required for

a 1,000 x 1,000 display, instead of 1,000,000 individual connections. For a flat panel display, the wiring is used to send signals from the computer graphics card to each display element. Where as in a detector the wiring is used to measure the signal generated in each detector element. The technology of the flat panel is 2 types, which direct detection and indirect detection. The flat panel used at chulalongkorn hospital is an indirect detection. Therefore, we only describe indirect detection flat panel systems.

3.10 Indirect Detection Flat Panel System[13]

Indirect flat panel detectors are sensitive to visible light, and an x-ray intensifying screen (typically Gd_2O_2S or CsI) is used to convert indirect incident x-rays to light, which is then detected by the flat panel. The term "indirect" comes from the fact that x-rays are absorbed in the screen, and the absorbed x-ray energy is then relayed to the photodetector by visible light photons. This indirect detection strategy is analogous to a screen-film system; expect that the electronic sensor replaces the light-sensitive film emulsion. Dual-emulsion film is thin and x-ray penetrates it easily; therefore, in a screen-film cassette, the film is sandwiched between screens to reduce the average light propagation path length and improve spatial resolution. Flat panel are thicker than film and do not transmit x-ray well; consequently, a sandwiched design is not possible. Instead, the intensifying screen is layered on the front surface of the intensifying screen strikes the flat panel, and much of the light that is released in the screen has to propagate relatively large distance through the screen, which results is more blurring. To improve this situation, most flat panel detector systems for general radiography use CsI screens instead of Gd_2O_2S. CsI is grown in columnar crystals, and the columns act as light pipes to reduce the lateral spread of light.
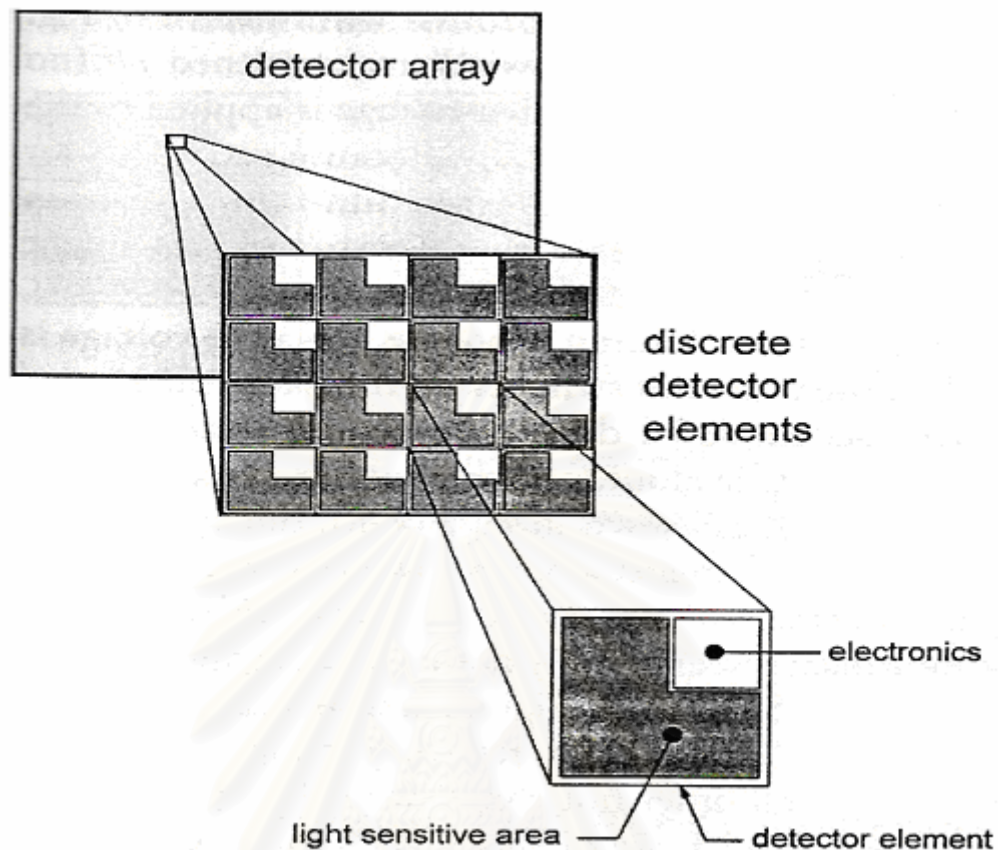
Figure 3.9 A flat panel detector array comprises a large number of discrete
detector elements. Each detector element contain both a light-sensitive
area and a region that holds electronic components

A typical configuration for a flat panel detector system is show in fig 3.9. The
flat panel comprises a large number of individual detector elements, each one capable
of storing charge in response to x-ray exposure. Each detector element has a light-
sensitive region, and a small corner of it contains the electronics. Just before
exposure, the capacitor, which stores the accumulated x-ray signal on each detector
element, is shunted to ground, dissipating lingering charge and released in the
photoconductor region on exposure to visible light. During exposure, charge is built
up in each detector element and is held there by the capacitor, after exposure, the
charge in each detector element is readout electronics as illustrated in fig 3.10.
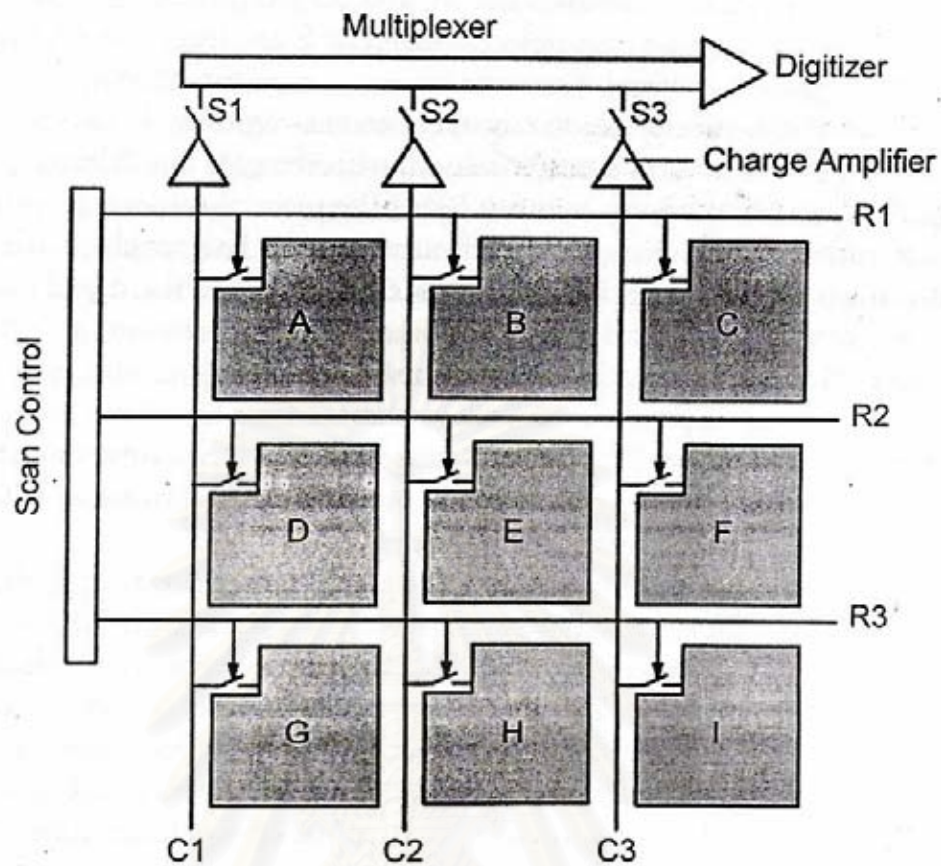
Figure 3.10 The process used for flat panel detector arrays.

From the fig 3.10, nine detector elements are shown (A through I). Three gate lines (row R1, R2, and R3) and three readout lines (columns C1, C2, and C3) are illustrated. A transistor is a simple electronic switch that has three electrical connections the gate, the source, and the drain. Each detector element in a flat panel detector has a transistor associated with it; the source is the capacitor that stores the charge accumulated during exposure, the drain is connected to the readout line (vertical wires in fig 3.10), and the gate is connect to the horizontal wires shown in fig 3.10. Negative voltage applied to the gate causes the switch to be turned off (no conduction from source to drain), whereas when a positive voltage is applied to the gate the switch is turn on (source is connected to drain). Because each detector element has a transistor and the device is manufactured using thin-film deposition technology, these flat panel systems are calling thin-film transistor (TFT) image receptors.

The readout procedure occurs as follows. During exposure, negative voltage is applied to all gate lines, causing all of the transistor switches on the flat panel imager to be turned off. Therefore, charge accumulated during exposure remains at the capacitor in each detector element. During readout, positive voltage is sequentially applied to each gated line (e.g., R1, R2, R3, as shown in fig 3.10), one gate line at a

time. Thus, the switches for all detector elements along a row are turned on. The multiplexer (top of fig 3.10) is a device with a series of switches in which one switch is opened at a time. The multiplexer sequentially connects each vertical wire (e.g., C1, C2, C3), via switches (S1, S2, S3), to the digitizer, allowing each detector element along each row to be read out. For example, referring to fig 3.10, when wire R2 is set to a positive gate voltage (all other horizontal wires being negative), the switches on detector elements D, E, and F are opened. Therefore, current can in principle flow between each of these detector elements (source) and the digitizer (drain). In the multiplexer, if the switches S1 and S3 are turned off and S2 is on, then the electrons accumulated on detector element E are free to flow (under the influence of an applied voltage) from the storage capacitor, through the charge amplifier, through the multiplexer (S2 is open) to the digitizer. Thus, the array of detector elements is read out in a raster fashion, with the gate lines selecting the row and the multiplexer selecting the column. By this sequential readout approach, the charge from each detector element is read out from the flat panel, digitized, and stored, forming a digital image. Notice that in this procedure the signal from each detector element does not pass through any other detector element, as it does in a needs only to by good (approximately 98%), whereas for a CCD the charge transfer efficiency needs to be excellent (greater than 99.99%). Therefore, flat panel systems are less susceptible to imperfections that occur during fabrication. This translates into improved manufacturing cost efficiency.

The size of the detector element on a flat panel largely determines the spatial resolution of the detector system. For example, for a flat panel with 125 x 125 μm pixels, the maximum spatial frequency that can be conveyed in the image (the Nyquist frequency, F_N) is $(2 \times 0.125 \text{ mm})^{-1}$, or 4 cycles/mm. If the detector elements are 100 μm, then $F_N = 5$ cycles/mm. Because it is desirable to have high spatial resolution, small detector elements are needed. However, the electronics (e.g., the switch, capacitor, etc.) of each detector element takes up a certain (fixed) amount of the area, so, for flat panel with smaller detector elements, a larger fraction of the detector element's area is not sensitive to light. Therefore, the light collection efficiency decreases as the detector elements get smaller. The ratio of the light-sensitive area to entire area of each detector element is called the fill factor (fig 3.11). It is desirable to have a high fill factor, because light photons that are not detected do not contribute to the image. If a sufficient number of the light photons generated in the intensifying screen are lost owing to a low fill factor, then contrast resolution (which is related to the signal-to-noise ratio) will be degraded. Therefore, the choice of the detector element dimensions requires a tradeoff between spatial resolution and contrast resolution.
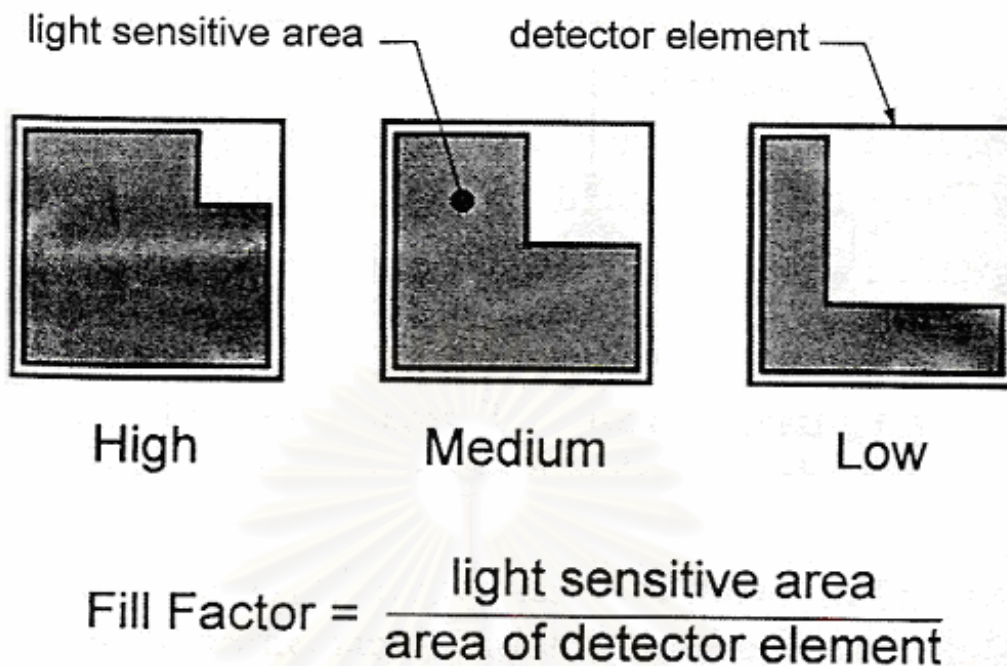
Figure 3.11 Fill factor

3.11 Acquisitions Mode in Flat Panel Detector[14,15]

Flat panel detectors generate frames either using free running or external triggered. The free running means that the camera sends out continuous frames according to the selected frame time. The external triggered means that there is an external trigger which allows the generation of the maskable interrupt request. All of the following acquisition modes are using external trigger and this trigger is generated by the linear accelerator and synchronize the image acquisition with linac. The following acquisition modes are implemented; Single mode, Cone Beam mode, and Continuous mode.

3.11.1 Single Mode-Low Dose Imaging

This control mode is used for verification of patient position. In this mode, sensors integrate the signal during the radiation interval and the data readout is performed after elapse of radiation. The detector is set in the external mode. The sensors are forced to be discharged prior to the start of radiation (Rad-on) to eliminate the dark current accumulation (fig 3.12). When the Rad-on signal is high, this means radiation is on and when the radiation is turned off, the Rad-on signal goes low. Three trigger pulses (3 frames scan) are sent to the external trigger input of the flat panel detector prior to the start of radiation (Rad-on signal) to force sensor discharge by reading 3 frames in absence of radiation. No readout is allowed during the radiation exposure interval. The trailing edge of the Rad-on signal, which corresponds, to

Radiation Off generates one trigger pulse (or 2 trigger pulses) and this initiates one frame (or couple of frames) readout and the accumulated data of the pixels during exposure interval is readout (data pulse). Forcing sensor discharge reduces the dark current accumulation prior to the start of radiation and therefore, reduces the image noise. Also, avoiding readout during radiation or exposure interval improves the image SNR by reducing the effect of the electronic readout noise, which is the dominant noise for low dose imaging. The other advantage of the readout after radiation exposure is the removal of the linac pulsing artifacts from the image.
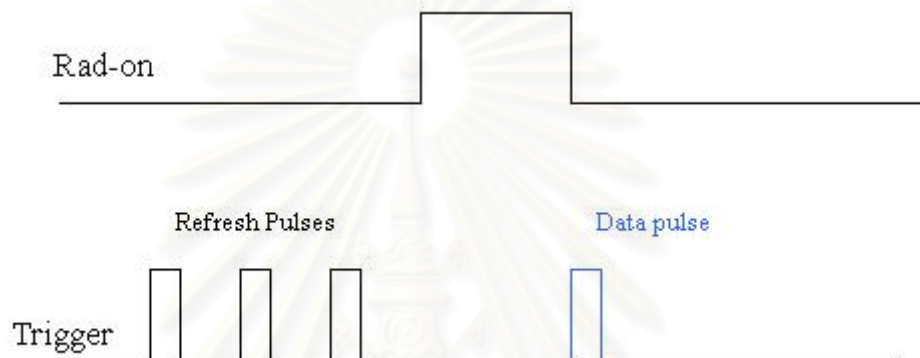
Figure 3.12 Single Mode with Forced Sensor Discharge

3.11.2 Continuous Mode-High Dose Imaging

This mode is mainly used for IMRT and monitoring the patient during the treatment and includes the movie images and verification image (average of movie images). This mode can be implemented using free running mode or external trigger mode. During free running mode, there is no synchronization between frame readout and linear accelerator and therefore, the linac pulsing artifacts cannot be removed by using free running mode. The external trigger continuous mode synchronizes the frame readout with linac pulsing. This will remove the pulsing artifacts and will not only improve the image quality of movie images but increases the accuracy of dosimetric verifications for applications such as IMRT.

The external continuous mode itself can be divided to two synchronization modes; one is the line synchronization and the other is frame synchronization.

In line synchronization, each lines can be triggered and readout individually. Two line triggering scheme can be implemented; one detects the linac pulse and readout a fixed number of lines (or rows) and then wait to the next trigger (linac pulse). A delay from the linac pulse to the start of the first line readout is used to compensate the scintillator screen persistence or decay time. Depending on the period of the X- ray beam pulse, the number of readout lines can be configured to avoid line

readout during the beam pulsing. For instance, if the beam pulsing period is 4.34 ms, the line readout time is 520 ms and the allocated delay for scintillator persistence is 500 ms; up to 7 lines can be scanned before the next beam pulse occurs. The second scheme uses the external trigger input as Start/Stop signal, meaning that when the trigger is high it starts the line readout until the trigger goes low (stops readout). A stop command which occurs during a line readout scan(~520 ms), will not be affected until the completion of that line, therefore, in this scheme there is a need to stop the line readout at least 520 ms before the next linac pulse. In frame synchronization mode, the start of frame is synchronized with linac pulses. The sensors are forced to be discharged prior to the start of radiation (Rad-on) to eliminate the dark current accumulation (fig 3.12). Sensor discharge is performed by the refresh scan (fig 3.13) prior to Rad-on. The EPID image I(x,y) obtained from continuous frame averaging is thesefore (Eq. (3.1)):

$$I(x, y) = \frac{1}{N} \sum_{j=1}^{N} I_j(x, y) \quad\ldots\ldots\ldots\ldots(3.1)$$

where $I_j(x,y)$ is the jth image frame, and **N** is the total number of frames acquired.
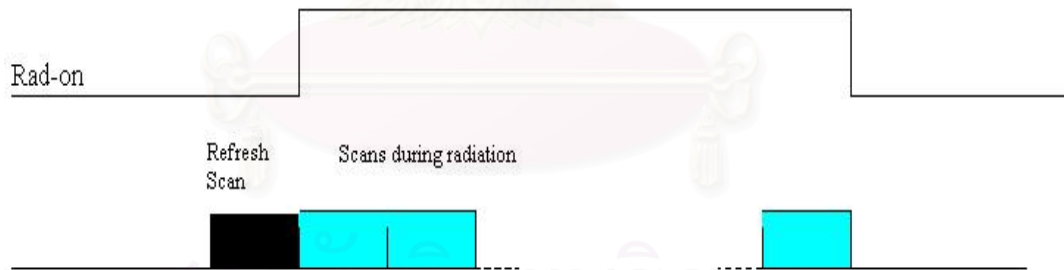
Figure 3.13 External Continuous Modes with Frame Synchronization

3.12 EPID Calibration[5,15]

The EPID is calibrated by the acquisition of dark-field (DF; fig 3.14) and flood field (FF; fig 3.15) images. The DF image is acquired with no radiation and records the pixel offsets. The FF image is recorded with an open field "uniform" irradiation to determine difference individual pixel sensitivities. When an image is acquired by the EPID the DF is subtracted and the image is then divided by the normalized FF image: the resulted image becomes uniform (fig 3.16).
The uniform image I(x,y) determined in (Eq. (3.2));

$$I(x,y) = \left(\frac{I_{raw}(x,y) - DF(x,y)}{FF(x,y) - DF(x,y)} \right) [FF(x,y) - DF(x,y)]_{mean} \quad ....(3.2)$$

Figure 3.14 The profile from dark field

Figure 3.15 The profile from flood field

Figure 3.16 The profile from EPID calibration

3.13 The aSi-based EPID[5,6,15]

The EPID used in research is a commercially available a-Si imaging device (aS500, Varian Medical Systems), mounted on a Clinac 23 EX (photon energies of 6 and 15 MV) with dynamic MLC (120 leaves) (Varian Medical Systems). The EPID system includes (i) an image detection unit (IDU), featuring the detector and accessory electronics, (ii) an image acquisition unit (IAS2), containing drive and acquisition electronics and interfacing hardware, and (iii) a dedicated workstation (PortalVision PC) located outside the treatment room. The IDU is essentially a matrix of 512 x 384 pixels with a resolution of 0.784 x 0.784 mm^2 and a total sensitive area

of, 40 x 30 cm^2. Each pixel consists of a light sensitive photodiode and a thin film transistor to enable readout. The electric charge generated by the incident photons is accumulated in the photodiode until the signal is read out and digitised through an analogue to digital converter. Overlying the array is a scintillating layer (gadolinium oxysulphide) and a copper plate (of, 1 mm thickness), making the portal imager an indirect detection system. The phosphor scintillator converts incident radiation into optical photons, enhancing the sensitivity of the detector more than tenfold. The total water-equivalent thickness of the construction materials in front of the photodiodes is 8 mm, as specified by the manufacturer. The IAS2 controls and reads the IDU. Its local hard disk contains the correction images (i.e. the dark and flood field acquisition) and the various acquisition parameter sets. In order to be able to detect all dose delivered to the portal imager during delivery of the treatment field, a special acquisition mode was used. During delivery, a continuous acquisition of frames is obtained. Each frame is read out line by line. The acquisition CPU (ACPU) contains a 14 bit A/D converter and is capable of adding 64 frames in its 20 bit hardware adder. Therefore, a transfer of the frame buffer to the CPU is mandatory after every 64th frame. This introduces a readout interrupt of ~ 0.164 s, as stated by the manufacturer and confirmed by our measurements. The interrupt occurs at regular time intervals of 64 times the acquisition time per frame (e.g. every 64 x 0.111 = 7.104 s for 300 MU/min). However, charge accumulation in the photodiode is not interfered with and it will thus not affect the final image accuracy, provided the accumulated charge between two subsequent readouts does not drive the 14 bit A/D converter into saturation.

3.14 EPID for Dosimetry in Dynamic Mode[6]

The conversion of the averaged gray-scale image into a PD image is done automatically in the dosimetric workspace of the PortalVision software. Firstly, it is multiplied by the total acquisition time. This time period, noted in the acquisition record, exceeds the beam-on time by 1–2 frame readouts as explained above. Secondly, a correction for the beam profile is applied. Although the standard dark field correction is applied, during the standard flood field calibration of the imager, the beam profile is assumed to be perfectly flat. This being a reasonable approximation for clinical imaging purposes, it introduces errors of a few percent into the dosimetric image. Hence it is corrected by means of a largest field profile as measured with ion-chamber in water phantom. The measured two-dimensional dose matrix was subsequently rescaled to SDD (source detector distance) = 145 cm, normalized to the beam axis and resampled to the detector grid, resulting in the field profile correction matrix. Thirdly, provided an absolute calibration of the imager has been performed, the image is multiplied with the calibration factor yielding what is referred to as the portal (PD) image. The PD image is expressed in calibrated units (CU). All PD image data used in this paper are obtained in this manner.

Furthermore, if not stated otherwise, all data were acquired with the commercially available detector as such, i.e. without any additional build-up placed onto the detector surface.

3.15 Portal Dose Image Prediction[6]

The aim of the pre-treatment verification of the dynamic IMRT fields by means of a portal imager is to assess the accuracy of the intended fluence as used in the TPS (Treatment Planning System) for dose calculation versus the actually delivered fluence through the dynamic leaf motion. Furthermore, the aim is to do so in an absolute way, making any additional (e.g. point dose) measurement unneeded. Since it is impossible to directly measure fluence with this detector system and detector response inevitably affects the incoming fluence measurement, a PD image prediction algorithm is mandatory to compare the theoretically expected measurement to the actual measurement.

The PD prediction algorithm for the a-Si measurement is based upon the single pencil beam dose calculation algorithm as originally developed by Storchi et al.[16] and as adapted into the Cadplan TPS (Varian Medical Systems) dose calculation and then adapted to Eclispe TPS. The PD prediction algorithm differs from the Eclispe algorithm in the sense that, in order to predict a fluence measurement with the portal imager, it uses beam data measurements with the portal imager rather than ionization chamber measurements in water. Furthermore, it does not require modelling of the depth dependence since we are focussing on image prediction at a fixed depth (i.e. in the commercially available portal imager as such).

In analogy to the single pencil beam algorithm in Eclispe, the absolute PD calculation per monitor unit can be separated into the phantom scatter and collimator scatter. Since the Varian MLC is a tertiary collimator, it can be considered as block replacement. Hence, the collimator scatter solely depends on the position of the main collimators. The scatter within the detector, i.e. the equivalent of the phantom scatter in the TPS dose calculation algorithm is determined by the incoming fluence distribution. The predicted PD image per MU (Moniter unit) for a field with collimator opening X, Y and intended, fluence f'(x; y; SDD) can then be written as Eq. (3.3)

$$P = f' \otimes k \cdot \left(\frac{SAD}{SDD} \right)^2 \cdot CSF_{XY} \quad \text{...............} \quad (3.3)$$

where

P $\qquad$ = Calculated portal dose image in term of CU

f' $\qquad$ = Input fluence corrected by the intensity profile and scaled by detector distance

$\otimes$ $\qquad$ = Convolution operator

k $\qquad$ = Portal imager dose kernel

SAD $\qquad$ = Source-to-axis distance of treatment unit

SDD   = Source-to-detector distance of the portal image

CSF$_{XY}$ = Collimator scatter factor

The open field fluence output of radiation devices is typically not uniform across the field. The dose image prediction compensates for the non-uniformity of the open beam fluence by modifying each pixel as in Eq. (3.4)

$$f'(x,y) = \frac{f(x,y)v(r_{x,y})}{MU_{factor}\max(f_0)} \quad \text{...................... (3.4)}$$

where

f'   = Corrected actual fluence

x,y   = Coordinates of a point in the fluence

f   = Original actual fluence

v(r)   = Radially symmetrical intensity value

r$_{x,y}$ = Radial distance form the beam axis

MU$_{factor}$ = MU factor from the dose distribution, used to scale the fluence

max(f$_0$)   = Maximum optimal fluence value,, used to scale the fluence

$$CSF_{XY} = \frac{OF(fx_s, fx_y)}{PSF(fs_x, fs_y)} \quad \text{...................... (3.5)}$$

where

fs$_x$ = Field size at the SAD in the FY-direction

fs$_y$ = Field size at the SAD in the FY-direction

PSF(fs$_x$, fs$_y$) = Phantom scatter factor for the field size fs$_x$, fs$_y$, defined at SAD

OF(fs$_x$, fs$_y$)   = Output factor for the field size fs$_x$, fs$_y$, defined at SAD and
                normalized to a 10 x 10 cm^2 field

The imager distance at which the measurement is going to be performed must be known at the time of image prediction, since the theoretical fluence and the beam profile correction (i.e. $(SAD/SDD)^2$) need to be rescaled accordingly. The fluence distribution as produced by the TPS is defined at isocentre and has a resolution of 0.25 x 0.25 cm^2. The first term of Eq. (3.3) describes the effect of the detector response function k. It is the point spread function or the equivalent of the single pencil beam kernel describing phantom scatter in the TPS dose calculation. The second term is beam profile correction. The third term holds the collimator scatter factor (CSF), solely dependent on the collimator opening. The theoretical fluence matrix as generated by the leaf motion calculator in the Eclispe/Helios software is normalised so that the maximum fluence is equal to unity. A value 1 corresponds to the fluence that would be delivered with a fully open field. The MU factor in Eq. (3.4), like a wedge factor, is an efficiency factor describing the surplus beam-on time required due to the leaf motion. Therefore, the final image has to be divided by the MU factor in order to obtain the prediction per MU.

The collimator scatter factor cannot be measured by the portal imager in a direct way, but can be derived from the measured output factor and the calculated phantom scatter factor. The latter is derived from convolving the open beam fluence f' with k; and monitoring the resulting value on the central axis. The output factor OF_{XY} is normalised to the PD per MU of a 10 x 10 field at SDD = 100 cm, i.e. OF_{10x10} (100 cm); 0.01 CU.

Essential to the quality of the portal image prediction is the accurate modelling of the portal imager response function. We have opted to take the resolution of the actual fluence already into account when modelling the k: The optimal k was obtained through a least square fit of the PD prediction to a PD measurement of a test plan especially developed for this purpose. The test plan consists of a fluence distribution as produced by the leaf motion calculator from an artificially created pyramid-like optimal fluence matrix (fig 3.17). The analytical function describing the k as a function of radial distance r from the pencil beam is modelled as a sum of three Gaussian contributions.

$$k(r) = \sum_i a_i e^{-r^{2/2\sigma_i^2}} \qquad \text{(3.6)}$$

where

r   = distance from origin

During the fit procedure, the Gaussian parameters in Eq. (3.6) are adjusted iteratively until the difference between the predicted dose image (Eq. (3.3)) and the measured test image is minimised. We make use of the Fast Fourier transform to derive the optimal k: Since the use of Fast Fourier transform requires that both functions are in Cartesian coordinates of the same resolution, the k is sampled from the radially symmetric analytical function in Eq. (3.6) to match the resolution of the fluence

matrix rescaled to the correct SDD. This resampling is performed for every iteration in the fit procedure. Hence the optimal fit parameters inherently take the discretisation into account.
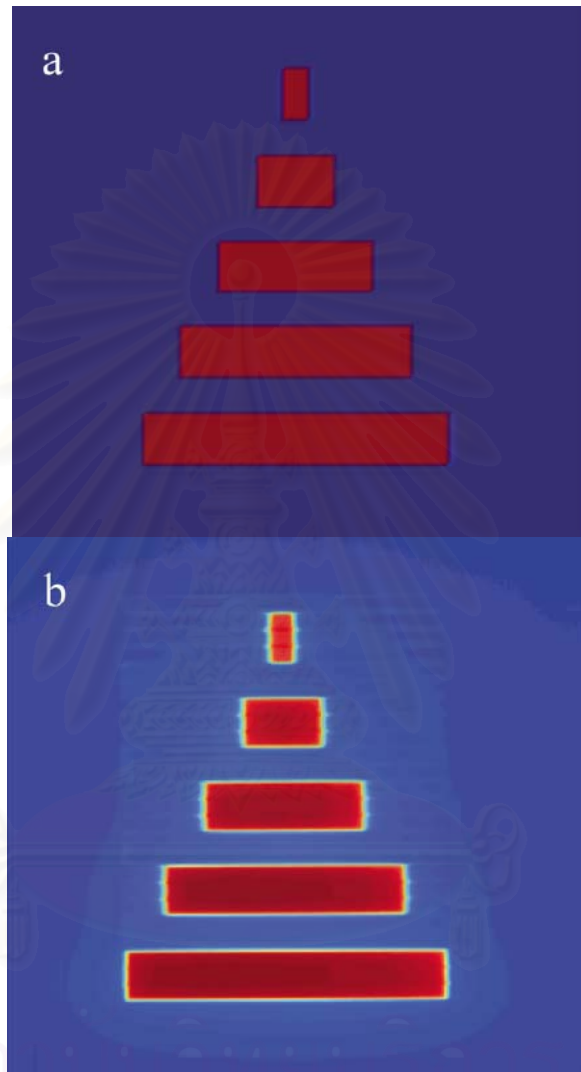
Figure 3.17 Pyramid-shaped theoretical test fluence pattern (a) and measured portal dose distribution (b) for the empirical derivation of the portal imager responsefunction.

CHAPTER IV

RESEARCH QUESTION AND RESEARCH OBJECTIVE

4.1 Research Questions

4.1.1 Primary research question

What dosimetric properties does the EPID show when compare with ion-chamber?

4.1.2 Secondary research question

Is it possible to use EPID to measure dose distribution of dynamic intensity modulated radiation therapy (IMRT) pre-treatment?

4.2 Research Objectives

1. To study the dosimetric properties of EPID.

2. To verify the dose distribution of IMRT pre-treatment using EPID.

CHAPTER V

RESEARCH METHODOLOGY

5.1 Research Design

This is an experimental study research.

5.2 Research Design Model

```
┌──────────────┐      ┌──────────┐      ┌──────────────────┐
│ Ion-chamber  │      │  EPID    │◄─────│ EPID calibration │
└──────────────┘      └──────────┘      └──────────────────┘
         │
         ▼
┌────────────────────────────────────┐      ┌──────────────┐
│ Different parameters influential    │─────►│  Field size  │
│ EPID as a dosimetry                 │      └──────────────┘
└────────────────────────────────────┘
         │                                   ┌──────────────┐
         ▼                              ────►│  Dose rate   │
┌────────────────────────────────────┐      └──────────────┘
│ Radiation dose measurement in      │
│ relative dose                       │      ┌──────────────┐
└────────────────────────────────────┘ ────►│     Dose     │
         │                                   └──────────────┘
         ▼
┌────────────────────────────────────┐      ┌──────────────┐
│ Different mechanical effects of     │─────►│  Dead time   │
│ EPID                                │      └──────────────┘
└────────────────────────────────────┘
         │                                   ┌──────────────┐
         ▼                              ────►│    Memory    │
┌────────────────────┐                       │    effect    │
│ EPID dosimetry     │◄──┐                   └──────────────┘
│ software           │   │
└────────────────────┘   │  ┌────────────────────┐
         │               └──│ EPID absolute      │
         ▼                  │ dose calibration   │
┌────────────────────────┐ └────────────────────┘
│ Beam profile           │      ┌──────────────┐
│ measurement            │─────►│  Open field  │
└────────────────────────┘      └──────────────┘
         │
         ▼                              ┌──────────────┐
┌────────────────────────────────────┐ │    Wedge     │
│ Verification of IMRT planning by   │►│    field     │
│ comparison between calculation and │ └──────────────┘
│ measurement                         │
└────────────────────────────────────┘
```

5.3 Key Word

- Electronic Portal Imaging Device (EPID)
- Intensity Modulated Radiation Therapy (IMRT)
- Amorphous Silicon
- Flat Panel Detector

5.4 Material

5.4.1 The linear accelerator

The Clinac 23EX linear accelerator used in the experiment is manufactured by Varian Oncology Systems, Palo Alto, CA, USA with dual photon beam of 6 MV and 15 MV, and six electron beam energies of 4, 6, 9, 12, 16 and 20 MeV. Photon field sizes are range from 0.3 x 0.3 cm^2 to 40 x 40 cm^2 at isocenter. The distance from the target to isocenter is 100 cm. These are five stationary therapy dose rates range from 100-600 monitor units per minute. The mulileaf collimator (MLC) is mounted below the conventional collimator in the same direction of X-jaws. There are 120 leaves that can move as the dynamic movement. We performed with a nominal beam dose rate of 300 MU/min.
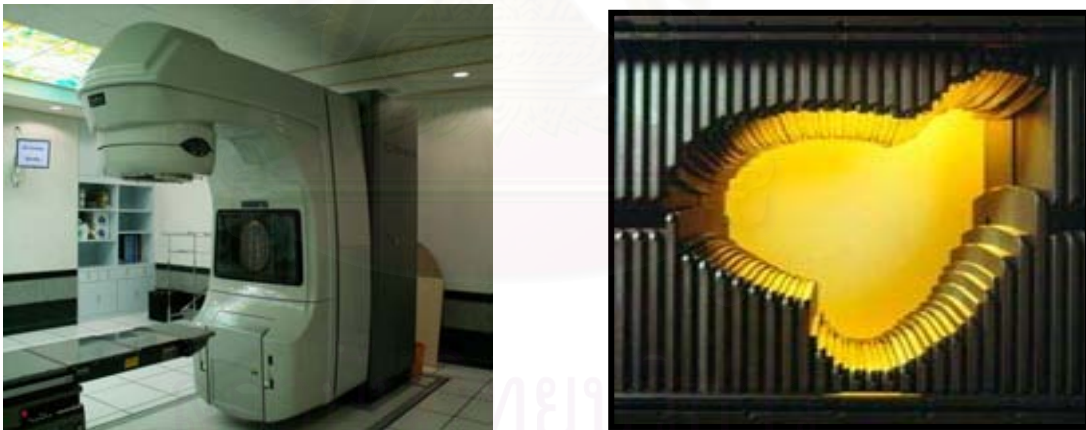
Figure 5.1 Linear accelerator (Clinac 23 EX) with
a dynamic multileaf collimator (DMLC).

5.4.2 Electronic Portal Imaging device (EPID)

The amorphous silicon EPID (aS500, Varian, Palo, CA) consists of a 1 mm copper metal plate, a 134 mg/cm^2 gadolinium oxysulphide phosphor screen (Kodak, Lanex Fast B) that includes a 0.18 mm polyester reflector, and a 40 x 30 cm^2 (512 x 384 pixel) a-Si array. Each pixel consists of a light sensitive photodiode and a thin-film transistor with a pixel pitch of 0.78 x 0.78 mm^2. The copper plate lies

beneath a 10-mm-thick foam layer with 1 mm of epoxy for binding. The scintillator and amorphous silicon array (~1mm thick) are bound to the underside of the copper plate and are enclosed between thin layers of black paper to prevent light scatter from the copper plate or components beneath the array, reaching the array. Beneath this lies a further 8 mm foam and 1 mm epoxy. A 1.6-mm-thick plastic collision cover (epoxy with glass and foam) encloses the detector with an air gap of approximately 1.5 cm between the cover and the detector surface. The EPID was integrated with a 6EX (6 MV) linear accelerator with a dynamic multileaf collimator (DMLC) with 1 cm leaf width.
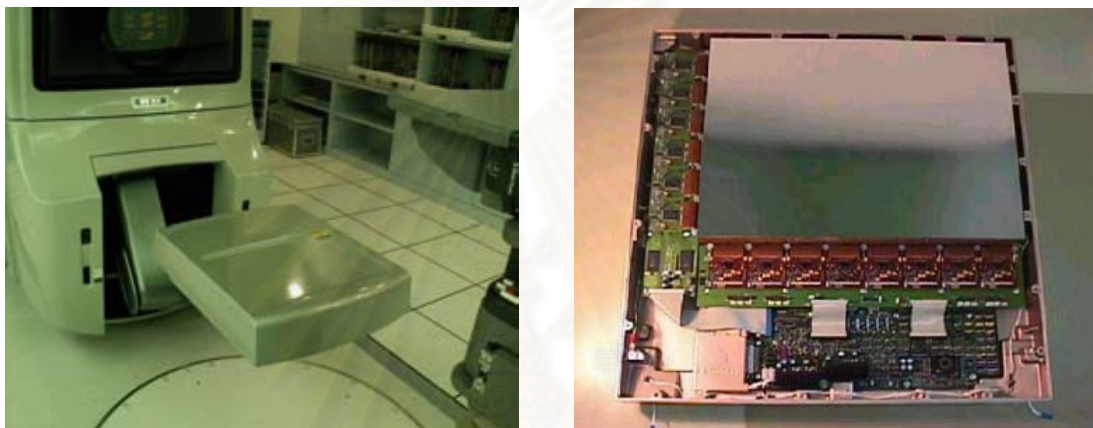
Figure 5.2 The amorphous silicon EPID (aS500, Varian)

5.4.3 AM maintenance program

The program is used for tuning and maintaining the PortalVision image acquisition system that can read line profile, pixel value, pixel region of interest, acquisition mode, time/frame and number of frames. Two possible modes of acquisition for the EPID systems are multiple image acquisition and continuous frame averaging. We used continuous mode for experiments because a single image consisting of average of the average of many image frames acquired during radiation delivery. The EPID will average successively acquired frames up to a limit of 9999 frames.

Figure 5.3 AM maintenance program

5.4.4 Eclipse integrated treatment planning

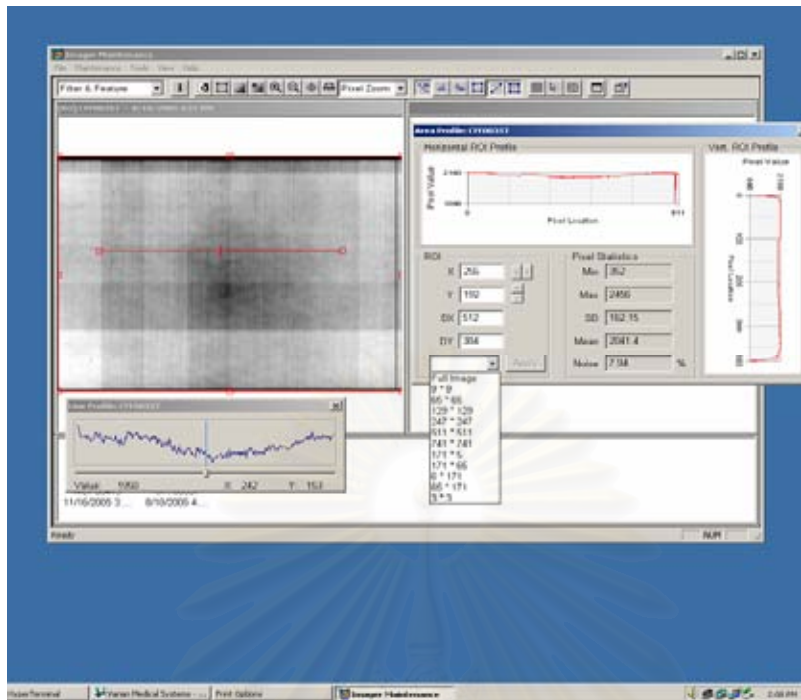Eclipse is a comprehensive system that simplifies the complexity of modern radiation therapy planning for all modalities such as 3D conformal, Intensity Modulated Radiation Therapy (IMRT), electron, proton, and brachytherapy. Advanced processes such as Image Guided Radiation Therapy (IGRT) and Dynamic Adaptive Radiation Therapy (DART) are supported. Eclipse helps dosimetrists, physicists, and physicians efficiently create, select, and verify the best treatment plans for their patients. Automation facilitates standards of care and protocols; yet, with the flexibility of Eclipse, the clinician can rapidly tailor plans for each patient. With Eclipse, efficiency and cost effectiveness for advanced techniques increase, providing true security of investment while improving the quality of care.

5.4.5 Portalvision aS500 program

PortalVision is an integrated part of the Clinac linear accelerator as well as the bridge between the treatments planning, record and verify, and QA processes. It allows you to verify the accuracy of the treatment plan before any prescribed dose is delivered to the patient. It facilitates accurate pre-treatment patient positioning prior to the first treatment session. And it provides ongoing verification of the accuracy of position during subsequent treatments, not merely before the prescribed radiation is turned on or after it is turned off. PortalVision's ability to image during treatment allows you to verify accurate positioning without increased dose to the patient. The

images become an important part of the documentation of accurate delivery of the prescription in the patient record.

5.4.6 Portal dosimetry mode

The portal dosimetry is consisted with Portal Vision hardware (EPID), acquisition module (4DTC/standalone PV), algorithm for dosimetric image prediction (Eclipse) and evaluation module (Review). This mode has environment options which integrated VMS environment (VARiS/Vision 6.5) and mixed environment. This mode is in dosimetry workspace that is available tools with point dose measurement, line dose measurement, isodose overlays, relative and absolute dose comparison, relative and absolute gamma evaluation.The pixel value in term of calibration unit (CU) is shown by dosimetry mode. This mode be able to see line profile, isodose chart and gamma evaluation for comparison with treatment planning system.
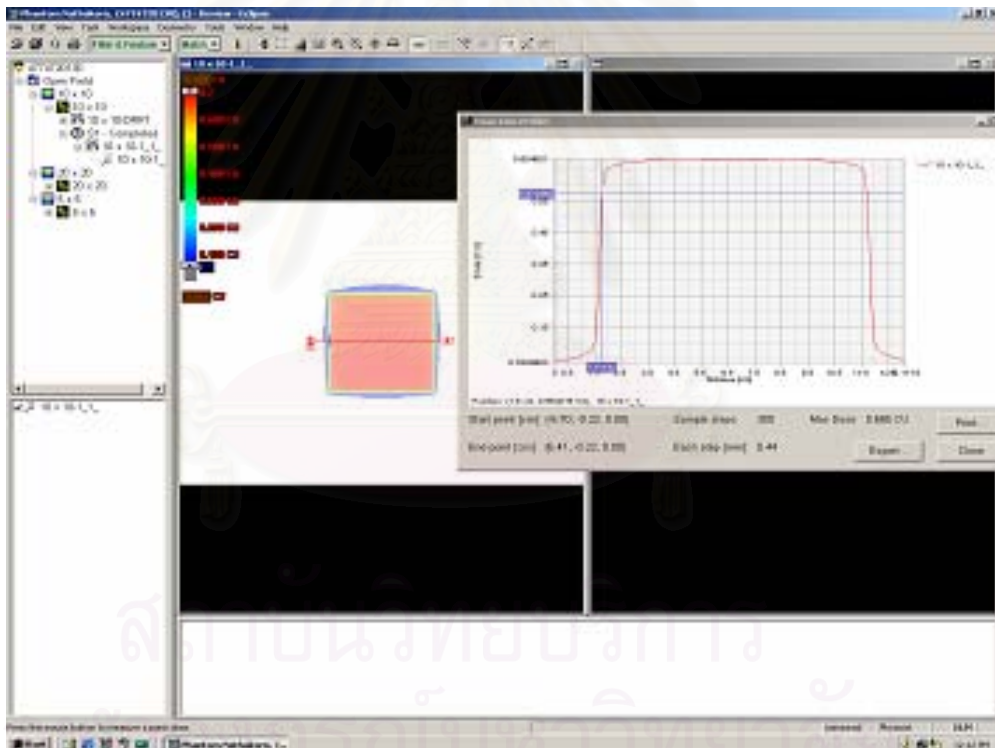

Figure 5.4 Portalvision aS500 program

5.4.7 Ion-chamber

The ion-chamber used in this study is the Scanditronix CC13 (0.125cc) compact chambers that can measure absolute and relative dosimetry of photon and electron beams in radiotherapy and can measure in solid phantoms or in water phantoms. The sensitivity of CC13 is 3.8×10^{-9} C/Gy.

Figure 5.5 0.125 cc ion-chamber (Well-hofer Dosimetrie,
Schwarzenbruck, Germany)

5.4.8 Electrometer

The DOSE-1 is a high-precision reference class electrometer that significantly exceeds the recommendations of the IEC 60731 and the AAPM ADCLs. It is suitable for the use with ion chambers, semiconductors and diamond probes. The DOSE-1 is ergonomically designed and intuitively easy to use. The standard DOSE-1 connects to either TNC or BNC connector types. Alternatively, the DOSE-1 is compatible with TNC, BNC, M-type and BNC/banana connector types. This electrometer was used with 0.125 cc ion-chamber and was setted at 300 V. Maximum charge per pulse is approximate $\pm$ 40 nC/pulse

Figure 5.6 DOSE-1 dosemeter

5.4.9 Phantom

5.4.9.1 The MedTec solid water phantom (density = 1.03 g/cm^3, atomic number = 5.97) is made in square slab of 30 x 30 cm^2 with the thickness of 0.2, 1.0 and 5.0 cm.

5.4.9.2 The Blue phantom (Scanditronix Wellhofer Dosimetric, Schwarzenbruck, Germany) is made from acrylic plastic (Perspex), having the scanning volume of 48 x 48 x 48 cm^3.

Figure 5.7 Solid water phantoms   Figure 5.8 Water phantom

5.4.10 Wedge filter

The wedge filter for the experiment is Varian's hard wedge type that is mounted on optical coded tray. It can be inserted in a four-way direction. We used 45 and 60 degree for the experiments.
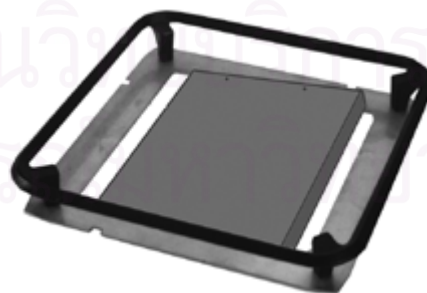

Figure 5.9 Wedge filter

5.5 Method

The study performed at department of radiology, King Chulalongkorn Memorial hospital was divided into 3 parts.

5.5.1 EPID calibration

5.5.1.1 EPID calibration in AM maintenance
5.5.1.2 EPID calibration in portal dosimetry

5.5.2 Parameters influence EPID dosimetry

5.5.2.1 The response of EPID with field size
5.5.2.2 The response of EPID with dose rate
5.5.2.3 The response of EPID with dose
5.5.2.4 Effect of dead time related to leaf speed in frame acquisition in dynamic field
5.5.2.5 Response to dose-rate fluctuations
5.5.2.6 Memory effect

5.5.3 EPID dosimetry

5.5.3.1 Relative dose measured for open and wedge fields
5.5.3.2 IMRT pre-treatment verification

5.5.1 EPID calibration

5.5.1.1 EPID calibration in AM maintenance

The EPID was calibrated by the acquisition of dark field and flood field. The calibration field size was 40 x 30 cm^2 at isocenter with the detector at a source detector distance (SDD) of 140 cm.

5.5.1.2 EPID calibration in portal dosimetry

The detector was calibrated to yield a PD of 1 CU for a 10 x10 cm^2 field size and a dose of 100 MU at SDD = 100 cm. Since in practice, the SDD cannot be reduced beyond 105 cm when the robotic arm is in clinical mode, the actual calibration was performed at SDD = 105 cm, setting the PD to be 0.90702 CU (i.e. assuming inverse square law behavior).

5.5.2 Parameters influence EPID dosimetry

5.5.2.1 The response of EPID with field size

In this experiment, the EPID was irradiated with 50 MU and the field size were varied from 4 x 4, 6 x 6, 8 x 8, 10 x 10, 12 x 12, 15 x 15, 18 x 18, 20 x 20 and 24 x 24 cm^2, respectively . The EPID was used in AM maintenance program, with 10 fixed frames mode. At each field size, three images of a field size are acquired and the mean pixel values in a 9 x 9 pixel region at the center of field size were recorded. To determine the relation of dose with field size; the ion-chamber is placed in a solid water phantom at SDD 105 cm, 1.5 cm depth with 5 cm of backscatter at each field size. Both measurements were normalized to the 10 x 10 cm^2 values.

5.5.2.2 The response of EPID with dose rate

In order to find the relationship between the signal and dose rate, irradiated EPID with 100 MU at 10 x 10 cm^2 field size. The changes in dose rate were the results of changes with SSD (100, 105, 120.2, 130.2, 140 and 151.2 cm). The EPID was used in AM maintenance program, with 10 fixed frames mode. At each distance, three image of a 10 x 10 cm^2 field size are acquired and the mean pixel values in a 9 x 9 pixel region at the center of field size were recorded. To determine the relation of dose rate with distance; the ion-chamber was placed in a solid water phantom at a 3.0 cm depth at each SDD.

5.5.2.3 The response of EPID with dose

Normally, the total dose in terms of pixel values can be found by the average pixel values multiplied by frame number. The experiment was performed at 4 x 4, 10 x 10 and 20 x 20 cm^2 field size with the varied dose of 10, 20, 30, 40, 50, 100, 150 and 200 MU. EPID was set at 105 cm SDD. The EPID was used in AM maintenance program with continuous mode. At each field size, three images are acquired and the pixel values were recorded from the mean pixel values in a 9 x 9 pixel region at the center of field size.

5.5.2.4 Effect of dead time related to leaf speed in frame acquisition in dynamic field

Sliding window deliveries were performed with a uniform 1 cm leaf gap between two banks of multileaf collimator (MLC) and a 10 x 10 cm^2 field size (fig 5.9). The speed of the MLC depended on the MU. The MU used was 50, 100 and 200, so the speeds of MLC were 1.0, 0.5 and 0.25 cm/s, respectively. Reduction in signal from a uniform profile occurred due to dead time in frame acquisition was quantified for each leaf speed. To determine error for each leaf speed in EPID, the X profile for each MU were compared. Profiles were obtained along the direction of leaf motion directly under the center of the MLC leaf adjacent to the central axis. The dropping of the profile near the end of the field represented the effect of the dead

time. The EPID was used in AM maintenance program, with continuous mode experimentation.
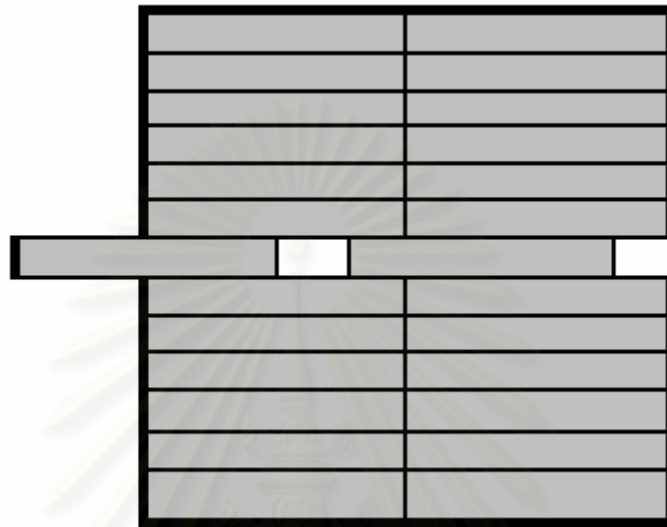

Figure 5.10 The sliding window with 1 cm leaf gap

5.5.2.5 Response to dose-rate fluctuations

The readout of the amorphous silicon array is synchronized with the beam pulses. The EPID was calibrated at 300 MU/min. The DF and FF images are different for each dose rate due to variation in the dose rate and image acquisition timing. During IMRT treatment, a large dose rate fluctuation may occur. These could affect the EPID signal where the EPID system is designed and calibrated with a fixed accelerator dose rate.

The effect was examined by recording a 'step-wedge' IMRT pattern (fig 5.10), which was 8 x 8 cm^2 field size. The dose setting was 50 MU and 500 MU. The Beam profile between 50 MU and 500 MU were obtained from EPID and compared.
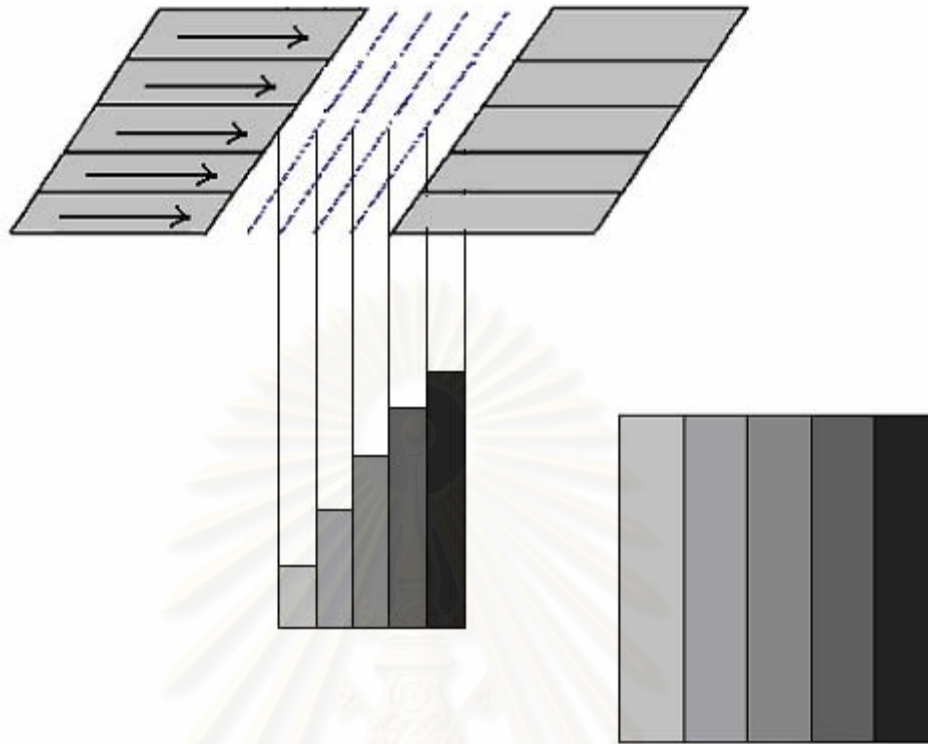
Figure 5.11 Step-wedge IMRT bar pattern

5.5.2.6 Memory effect

An image was acquired with a 4 x 4 cm^2 field size, followed immediately by an image of a 10 x 10 cm^2 field size. The interval between the two images was approximately 15 s. A memory effect of the EPID will manifest as an increase in the pixel value for the 10 x 10 cm^2 field size in the region of irradiation of the 4 x 4 cm^2 field size. An image was acquired of the 10 x 10 cm^2 field after several minutes had elapsed of the comparison (fig 5.11). The area 4 x 4 cm^2 at the center of the 10 x 10 cm^2 field size images were compared to see whether the pixel values were elevated due to a memory effect.

Figure 5.12 The 10 x 10 cm^2 field size with and without memory effect

5.5.3 EPID dosimetry

5.5.3.1 Relative dose measured for open and wedge fields

The beam profiles from EPID were compared with the profile measured from ion-chamber. Images were acquired with 4 x 4, 10 x 10 and 20 x 20 cm^2 field size (fig 5.13). The EPID was at 105 cm from source. The next step was to test 45 and 60 degrees wedge filter of 4 x 4, 10 x 10 and 20 x 20 cm^2 field size (5.14). These experiments have been performed in portal dosimetry mode. Then EPID profiles through the central axis of open and wedge fields were compared with Ion-chamber measured at 1.5 cm depth in a water phantom at 100 cm SSD. The EPID data were scaled to 101.5 cm for comparison.
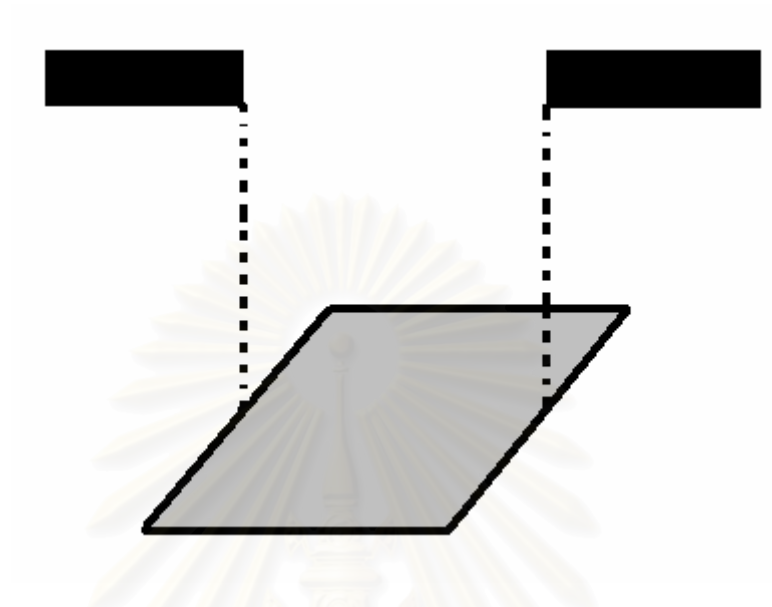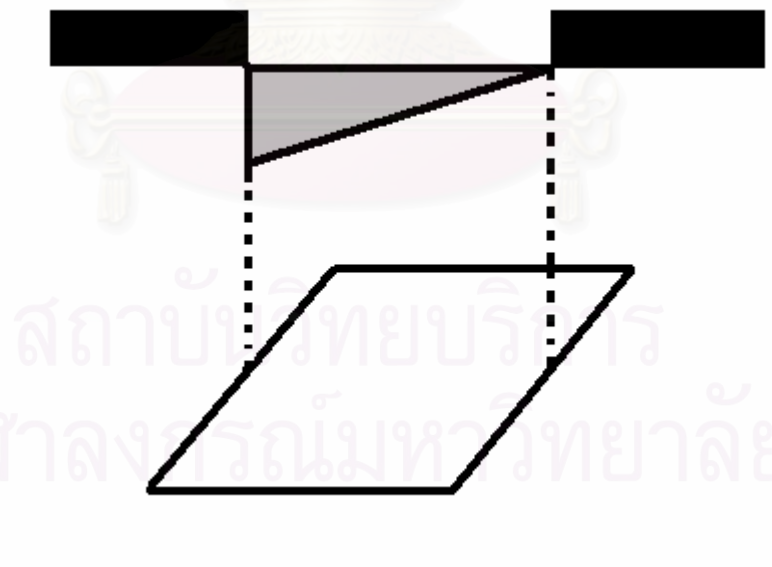
Figure 5.13 Open field

Figure 5.14 Wedge field

5.5.3.2 IMRT pre-treatment verification

For pre-treatment verification of the IMRT fluence, 2 images of clinical IMRT field of CA-Naspharynx were taken without the patient. The predicted isodose distribution calculated by treatment planning was compared with the isodose measured from EPID. The gamma value of 3% difference in percentage depth dose and 3 mm difference in distance were selected for analyzing the result. Profiles in the leaf motion direction were compared at the central axis and at off-axis planes

5.6 Measurement

| Independent variables | = | the properties of EPID are dose linearity, sampling of rapid multileaf collimator (MLC) leaf speeds, response to dose rate fluctuations, memory effect, and Relative dosimetry |
| Dependent variables | = | the pixel value of image is shown by EPID measurement |

5.7 Data collection

The performance of the amorphous silicon detector is assessed for pre-treatment dosimetric measurement of IMRT beam delivery. Image acquisition for IMRT verification is performed by acquiring a single image comprised of multiple image frames, and then a single image is the average of all the image frames. The values in the experiment are measured by determining mean (acquired from 3 images) of the pixel values in 9 x 9 pixel region at the center of the field. Finally, determine the point doses and profiles with ion-chamber in water phantom. All the data are presented in graphic form.

5.8 Data Analysis

5.8.1 Summarization of data

The pixel value and radiation dose are continuous data, the average are analyzed.

5.8.2 Data presentation

The result is shown in graphical form and table.

5.9 Expected Benefit and Application

- Verification of IMRT treatment.
- The ability of EPID to measure dose distribution instead of film.
- Quality assurance of MLC and beam parameters

5.10 Ethic Consideration

There are not ethical issues because the radiation dose is measured in phantom in this study.

CHAPTER VI

RESULTS AND DISCUSSION

6.1 EPID Calibration

The calibration of the EPID with a FF image is important for accurate signal response as all acquired images are divided by the normalized FF image. This image is acquired to correct for non-uniformities in the EPID response, and after calibration, the input beam profile for the FF acquisition is uniform. The image should be calibrated every month for high quality image[15].

6.2 Parameters Influence EPID Dosimetry

6.2.1 The response of EPID with field size

The EPID response in term of the mean pixel values in 9 x 9 pixel region at the center of field and ion-chamber reading with field size normalized to the 10 x 10 cm^2 values are shown in table 6.1 and the graphs are plotted in fig 6.1. Second-order polynomials were fitted to the data. Also shown in the graph is the EPID signal divided by the ion-chamber value. This graph illustrated the deviation of EPID response from ion-chamber response. The EPID response was shown the error of 4.09% for a 4 x 4 cm^2 and 4.90% for a 24 x 24 cm^2 field size when compared with ion-chamber. The areas which were close to 10 x 10 cm^2 normalized field had less error.

Table 6.1 The mean EPID pixel values at various field sizes compared with ion-chamber in term of relative dose normalized to the response of 10 x 10 cm^2 field size

| Field size (cm^2)	Mean pixel values	Relative dose measured by EPID	cGy (ion-chamber)	Relative dose measured by ion-chamber	% deviation from ion-chamber
4 x 4	4,288.26	0.890	1.625	0.928	4.09
6 x 6	4,516.60	0.938	1.678	0.958	2.08
8 x 8	4,692.60	0.974	1.718	0.981	0.71
10 x 10	4,815.40	1.000	1.751	1.000	0.00
12 x 12	4,951.10	1.028	1.777	1.015	1.28
15 x 15	5,087.16	1.056	1.804	1.030	2.52
18 x 18	5,227.13	1.085	1.828	1.044	3.92
20 x 20	5,261.56	1.092	1.838	1.049	4.09
24 x 24	5,350.83	1.112	1.857	1.060	4.90
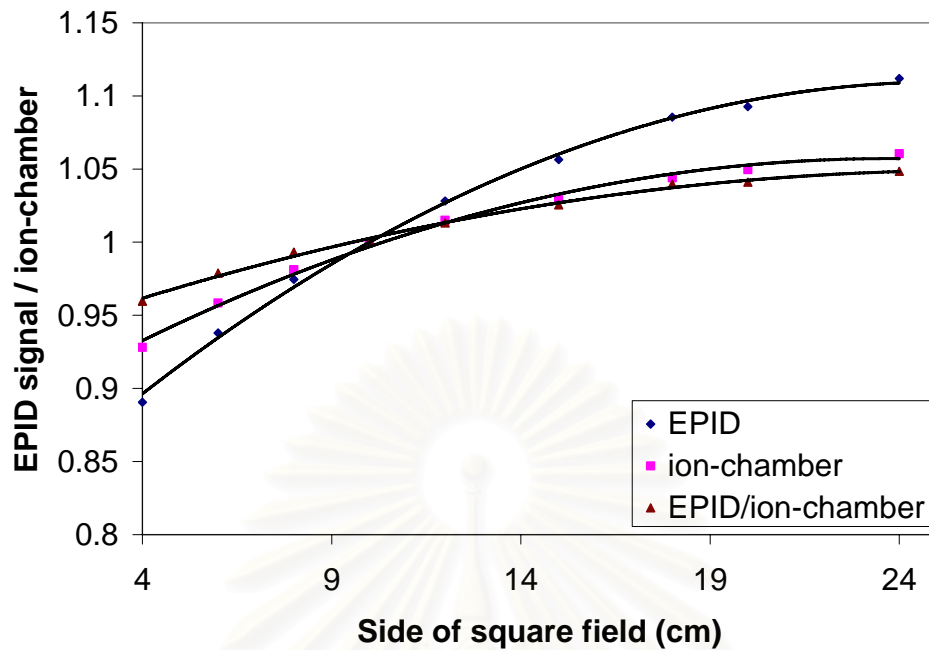
Figure 6.1 Field size dependence on the EPID and ion-chamber

The graph showed increasing in EPID and ion-chamber responses with field size which means that the scatter radiation was increasing when field size was increased. Since the scatter has a low energy component, its effect on the EPID's phosphor response for field size larger than 10 x 10 cm^2 was enhanced compared to ion-chamber due to the presence of high atomic number components in the phosphor. The response of EPID was less for small field size.

6.2.2 The response of EPID with dose rate

The relationships between the dose rate (MU/min) measured by ion-chamber and mean pixel values are shown in table 6.2 and the graph is plotted in fig 6.2. The linearity of the EPID with dose rate are shown with $R^2 = 1$. From this result, it can be seen that when the source surface distance was increased which mean that the dose rate was decreased, there would be a decrease in pixel values.

Table 6.2 The relation of mean EPID pixel values and dose rate (obtained by varying SSD) for 10 x 10 cm^2 field size.

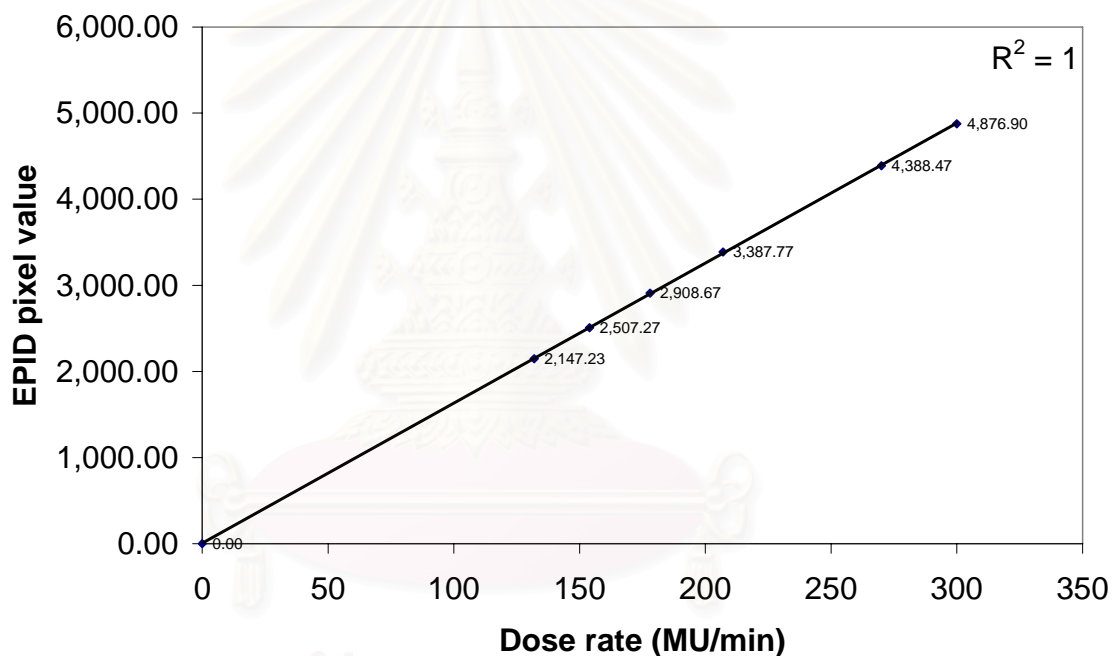| Source surface distance (cm)	dose rate (MU/min)	Mean pixel values
100.0	300	4,876.90
105.0	270	4,388.47
120.2	207	3,387.77
130.2	178	2,908.67
140.0	154	2,507.27
151.5	132	2,147.23

Figure 6.2 The linearity of the detector with dose rate for 10 x 10 cm^2 field size.

6.2.3 The response of EPID with dose

The linearity with integral dose had been reported in many researches[5,6,9]. The integral doses of EPID were obtained by multiplication of the pixel values by the number of frames. The experiment's result of the relationship between integral dose in term of MU and the mean values of EPID pixel values multiple by number of frames can be seen in tables 6.3, 6.4, and 6.5 for 4 x 4, 10 x 10 and 15 x 15 cm^2 field sizes, respectively. All of data were transformed into graph format shown in figure 6.3, 6.4 and 6.5. The linearity of the mean EPID pixel values multiplied by number of frames with integral dose at three field sizes of 4 x 4, 10 x 10 and 15 x 15 cm^2 are

shown with R^2 = 0.9998, 0.9979 and 0.9996, respectively. From the results, it can be seen that when doses were increased, there would be an increasing in pixel values and frames. All the field sizes studied showed the linearity of mean pixel values and frames with doses. During irradiation, if the dose rate was fluctuated, the pixel values would show slightly non-linearity with dose. When the mean pixel values multiplied by the frames, the result showed linearity with the dose. This due to the compensation of pixel values with the frame.

Table 6.3 The mean EPID pixel values multiplied by number of frames for different doses (MU) of 4 x 4 cm^2 field size.

Dose(MU)	Mean pixel values(P)	Frames(F)	P x F (x10^5)
10	3,889.8	14	0.54
20	4,041.1	32	1.29
30	4,132.7	50	2.06
40	4,143.0	65	2.69
50	4,148.1	83	3.44
100	4,185.1	170	7.11
150	4,196.7	256	10.74
200	4,238.9	334	14.15

Table 6.4 The mean EPID pixel values multiplied by number of frames for different doses (MU) of 10 x 10 cm^2 field size.

Dose(MU)	Mean pixel values(P)	Frames(F)	P x F (x10^5)
10	4,641.3	13	0.60
20	4,668.3	33	1.54
30	4,789.5	49	2.34
40	4,815.9	65	3.13
50	4,815.9	82	3.94
100	4,840.2	166	8.03
150	4,860.0	238	11.56
200	4,822.7	344	16.59

Table 6.5 The mean EPID pixel values multiplied by number of frames for different doses (MU) of 15 x 15 cm^2 field size.

Dose(MU)	Mean pixel values(P)	Frames(F)	P x F (x10^5)
10	4,531.8	15	0.67
20	4,763.1	34	1.61
30	5,456.5	40	2.18
40	4,804.5	72	3.45
50	5,163.2	82	4.23
100	5,107.9	173	8.83
150	5,509.5	238	13.11
200	5,273.1	335	17.66
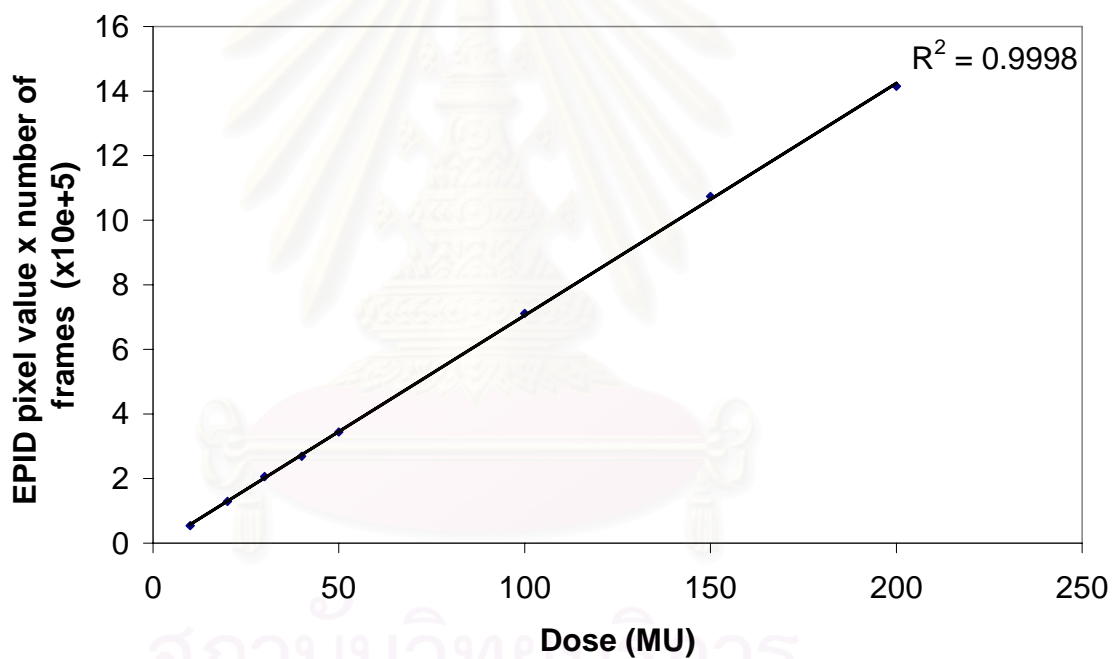
Figure 6.3 The linearity of EPID with integral dose in 4 x 4 cm^2 field size.

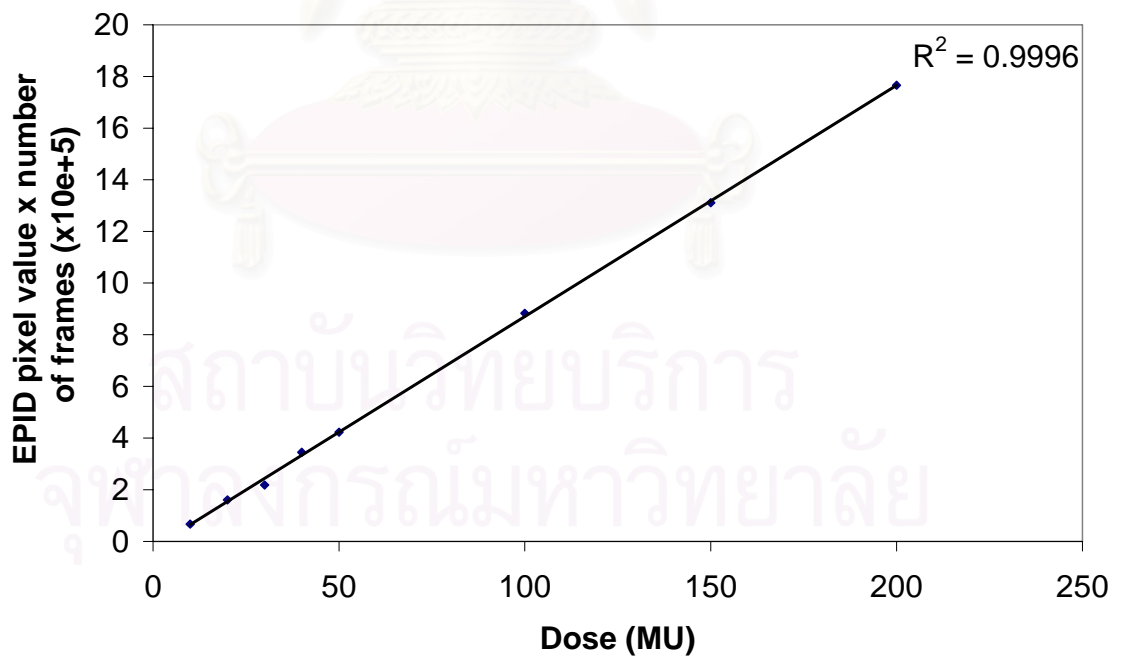Figure 6.4 The linearity of EPID with integral dose in 10 x 10 cm^2 field size.

Figure 6.5 The linearity of EPID with integral dose in 15 x 15 cm^2 field size.

The effect of dead time was occurred every 64 frames[5,6,15]. The result of the experiment showed that the effect of dead time started at 40 MU. The acquisition time per frame usually is 0.111 sec, therefore we can find the acquisition time per frame dealing with dead time by dividing the total acquisition time reading by number of frame reading. The results showed the acquisition time per frame of greater value than 0.111 sec when the dead time had been occurred. If there was no dead time, the number of frames would be the actual acquisition time divided by 0.111 sec. The frame without dead time showed higher value than the frame with dead time for the dose greater or equal to 40 MU. The frames without dead time multiplied by pixel value were higher when compared with the frame with dead time multiplied by pixel value as shown in table 6.6, 6.7 and 6.8 and shown in fig 6.6, 6.7, 6.8 for 4 x 4, 10 x 10 and 15 x 15 cm^2 field size, respectively. The error signal due to dead time increased when the dose was increasing and seem to be field size independent. So for the static field of 200 MU maximum doses, the error due to dead time of 4 x 4, 10 x 10 and 15 x 15 cm^2 field size were within 3.60%, 2.89% and 3.00%, respectively.

Table 6.6 The mean EPID pixel values multiplied by number of frames with and without dead time for difference dose (MU) of 4 x 4 cm^2 field size.

Dose (MU)	Mean pixel values (P)	Acquisition time reading (sec) (T)	Number of frames with dead time reading (F_d)	T/F_d	Number of Cal. frames without dead time (F_c)	P x F_d (x10^5)	P x F_c (x10^5)	Error with dead time (%)
10	3,889.8	1.554	14	0.111	14	0.54	0.54	0.00
20	4,041.1	3.552	32	0.111	32	1.29	1.29	0.00
30	4,132.7	5.550	50	0.111	50	2.06	2.06	0.00
40	4,143.0	7.215	65	0.111	65	2.69	2.69	0.00
50	4,148.1	9.379	83	0.113	85	3.44	3.52	2.32
100	4,185.1	19.380	170	0.114	175	7.11	7.32	2.95
150	4,196.7	29.440	256	0.115	265	10.74	11.12	3.53
200	4,238.9	38.410	334	0.115	346	14.15	14.66	3.60

Table 6.7 The mean EPID pixel values multiplied by number of frames with and without dead time for difference dose (MU) of 10×10 cm^2 field size.

Dose (MU)	Mean pixel values (P)	Acquisition time reading (sec) (T)	Number of frames with dead time reading (F_d)	T/F_d	Cal. Number of frames without dead time (F_c)	P x F_d (x10^5)	P x F_c (x10^5)	Error with dead time (%)
10	4,641.3	1.443	13	0.111	14	0.60	0.60	0.00
20	4,668.3	3.663	33	0.111	32	1.54	1.54	0.00
30	4,789.5	5.439	49	0.111	50	2.34	2.34	0.00
40	4,815.9	7.215	65	0.111	65	3.13	3.13	0.00
50	4,815.9	9.266	82	0.113	84	3.94	4.04	2.53
100	4,840.2	18.919	166	0.114	170	8.03	8.22	2.36
150	4,860.0	27.097	238	0.114	244	11.56	11.85	2.50
200	4,822.7	39.256	344	0.114	354	16.59	17.07	2.89

Table 6.8 The mean EPID pixel values multiplied by number of frames with and without dead time for difference dose (MU) of 15×15 cm^2 field size.

| Dose (MU)	Mean pixel values (P)	Acquisition time reading (sec) (T)	Number of frames with dead time reading (F_d)	T/F_d	Cal. Number of frames without dead time (F_c)	P x F_d (x10^5)	P x F_c (x10^5)	Error with dead time (%)
10	4,531.8	1.665	15	0.111	15	0.67	0.67	0.00
20	4,763.1	3.784	34	0.111	34	1.61	1.61	0.00
30	5,456.5	4.440	40	0.111	40	2.18	2.18	0.00
40	4,804.5	8.159	72	0.113	74	3.45	3.55	2.89
50	5,163.2	9.288	82	0.113	84	4.23	4.33	2.36
100	5,107.9	19.591	173	0.113	177	8.83	9.04	2.37
150	5,509.5	27.112	238	0.114	244	13.11	13.44	2.51
200	5,273.1	38.250	335	0.114	345	17.66	18.19	3.00
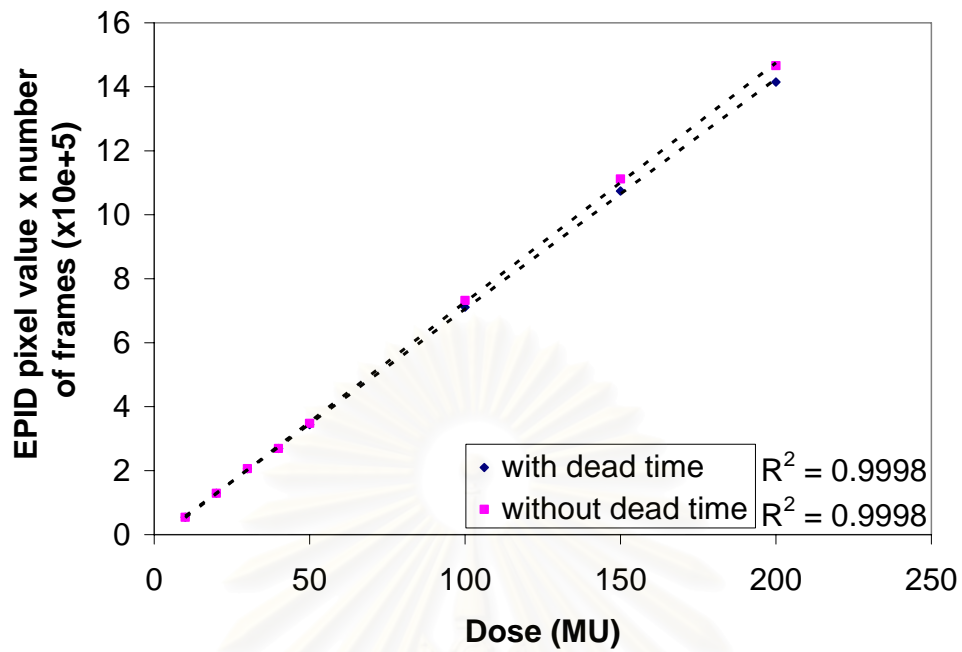
Figure 6.6 The linearity of integral dose in 4 x 4 cm^2 field size
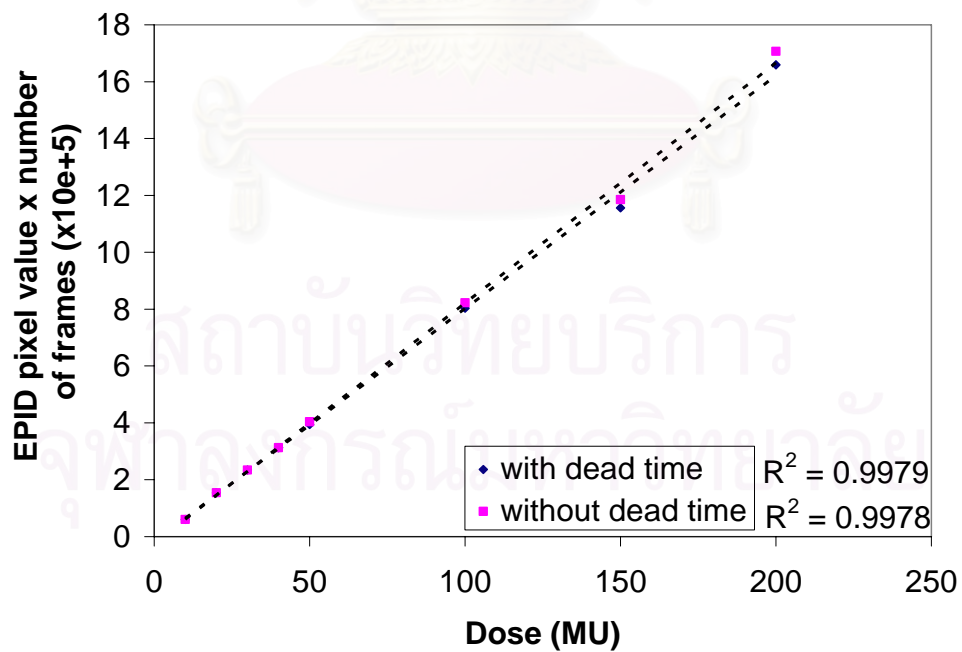with and without dead time.

Figure 6.7 The linearity of integral dose in 10 x 10 cm^2 field size
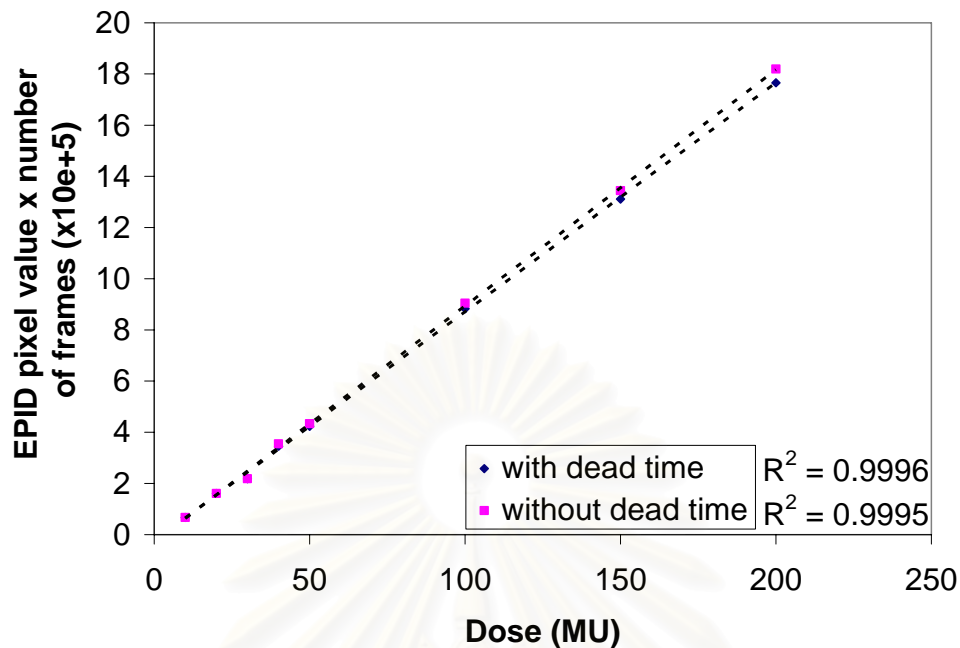with and without dead time.

Figure 6.8 The linearity of integral dose in 15 x 15 cm^2 field size
with and without dead time.

6.2.4 Effect of dead time related to leaf speed in frame acquisition in dynamic field

In the past study on the effect of dead times[5], it was found that during EPID read out in every 64 frames, there would be data transfer to the CPU (Center Process Unit), with total time loss of 0.28 seconds, which was equal to 2 frames losses. While the data were transferred, EPID will not be able to collect signals, even if radiation were still delivered. Due to effect of dead times, EPID will have loss some signal. The resulted of static field has been shown in 6.2.3 as mentioned.

Sliding window delivery with 0.25 cm/s leaf speed is shown as an example in fig 6.9. From fig 6.10, 6.11, 6.12, the profiles of the EPID are shown at various leaf speeds of 0.25, 0.5 and 1 cm/s which obtained by giving the dose of 200, 100 and 50 MU, respectively. The part of profile that shifts from the flat part represented the errors of each leaf speed. From this result, with the increase in lead speed, there would be an increase in signal errors, as seen in table 6.9. The highest signal error value was equal to 17.62% at leaf speed of 1 cm/s and the lowest error value was equal to 3.37% at leaf speed of 0.25 cm/s. Therefore in IMRT treatment, with high leaf speed, the profile could show a higher error signal in EPID. For accurate dosimetry in EPID, the leaf speed should be slower or with larger MU.
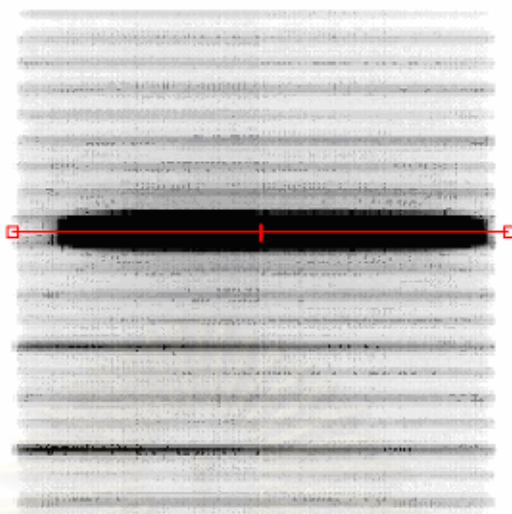
Figure 6.9 Sliding window delivery of EPID on x-axis
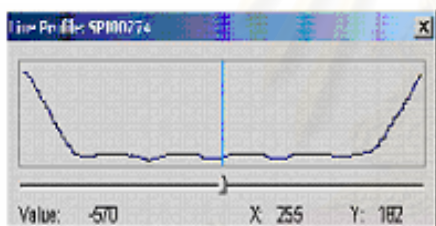with the effect of dead time

Figure 6.10 The profile of EPID
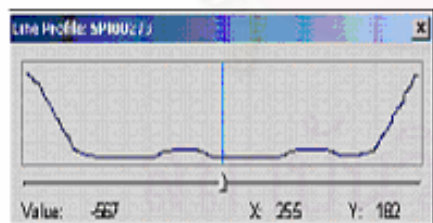at
0.25 cm/s leaf speed

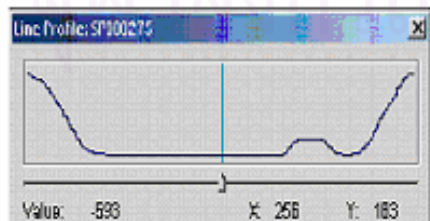Figure 6.11 The profile of EPID
at
0.50 cm/s leaf speed

Figure 6.12 The profile of EPID
at
1.00 cm/s leaf speed

Table 6.9 The signal error of EPID due to dead time when increasing the leaf speed

Leaf Speed (cm/s)	Dose (MU)	Pixel value without dead time	Pixel value with daed time	Error (%)
0.25	200	570.00	550.75	3.37
0.50	100	579.67	534.00	7.87
1.00	50	590.00	486.00	17.62
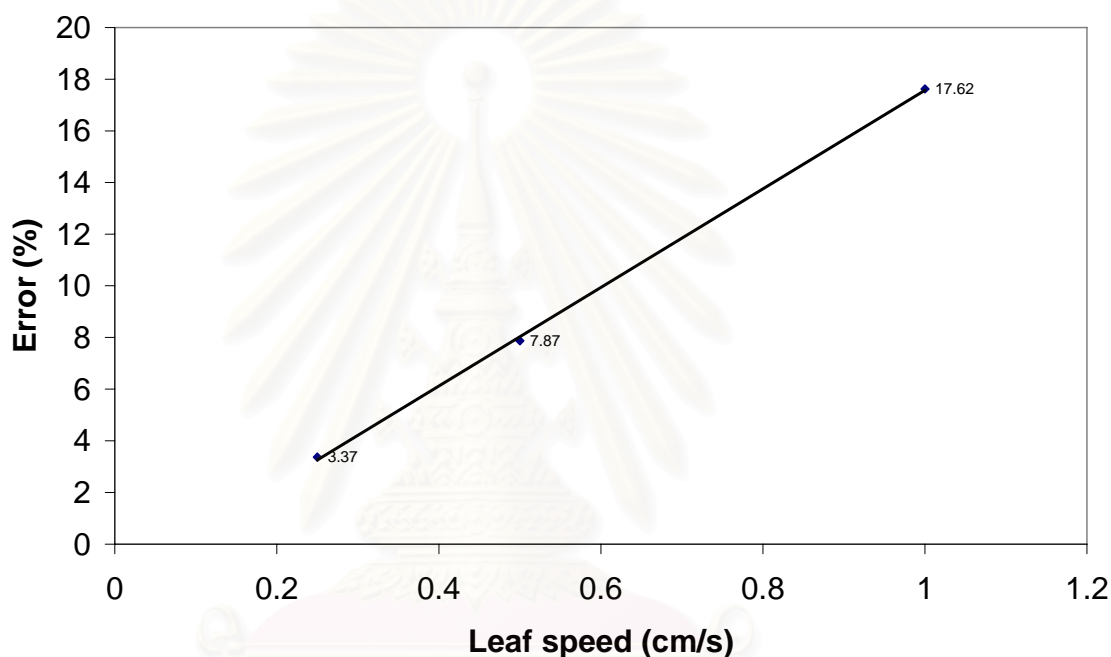
Figure 6.13 The percentage of error due to dead time when increasing the leaf speed

6.2.5 Response to dose-rate fluctuations

From DMLC characteristics on beam hold off, and from the Greer's research[5], it was found that in IMRT treatment, when the leaves have not reached the designated position with maximum leaf speed then beam hold off result where the accelerator reduces dose rate until the leaf desired position. This can result in large dose rate fluctuation during delivery.

The profiles with and without dose rate fluctuations are shown in fig 6.14 by the dose of 50 MU had beam hold off and 500 MU had not beam hold off. There was less than one percent differences between the two profiles in the areas where the beam hold off occurred.
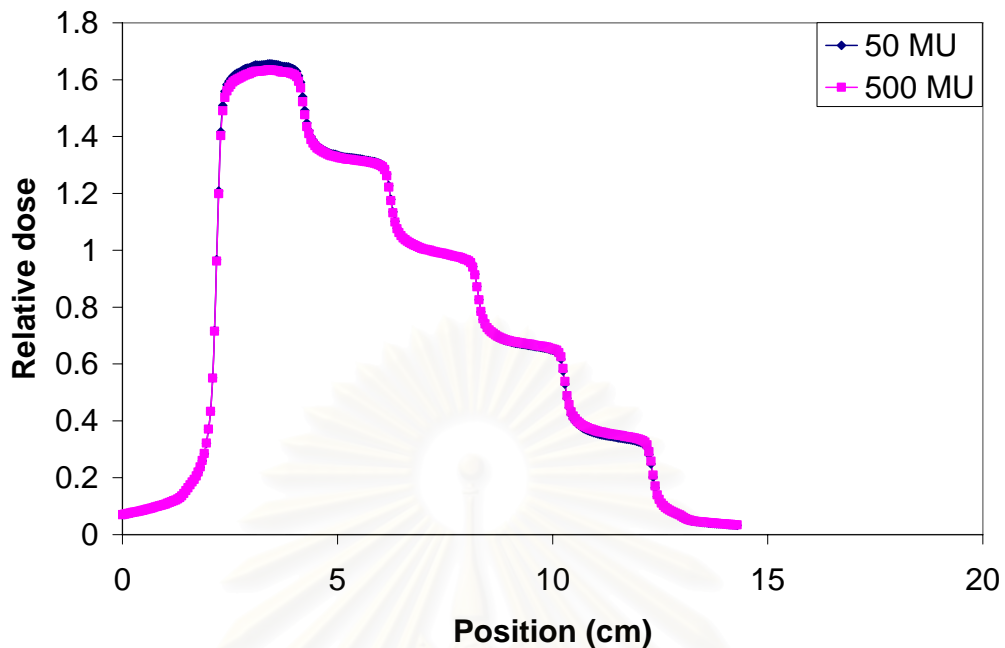
Figure 6.14 The profile of IMRT 'stepped wedge' with and without beam hold off

From the experiment it can conclude that the dose rate fluctuation have no effect with the readout of EPID. Therefore the synchronization of the readout in EPID with beam pulses was not effect for dosimetry.

6.2.6 Memory effect

The existence of a memory effect of the a-Si detector referred to a 'ghosting'. The ghost images[5,6,9] referred to the image of an object that was in the previous acquisitions and was presented in the next acquisition.

The profiles of 10 x 10 cm^2 field size of without ghost effect and the profile of ghost effect of 4 x 4 cm^2 field size followed in 15 sec with 10 x 10 cm^2 field size are shown in fig 6.15. They were obvious in area of 4 x 4 cm^2 field size which ghost effect occurred. The fig 6.15 was zoomed and shown in fig 6.16. In the area of 4 x 4 cm^2, the signal difference between ghost and without ghost effect was within 1.5%.
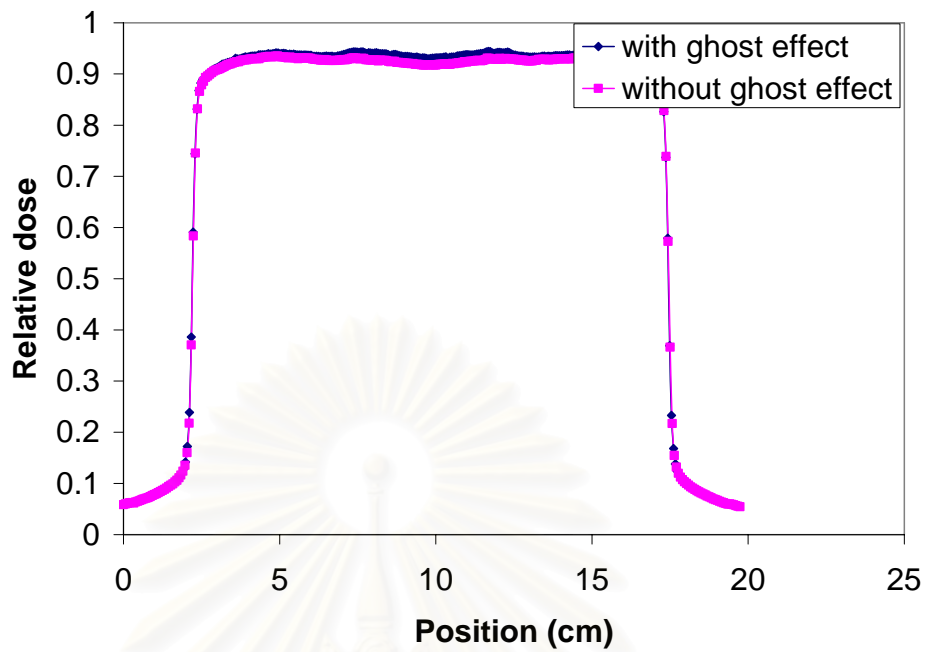
Figure 6.15 The profile of 10 x 10 cm^2 with and without ghost effect
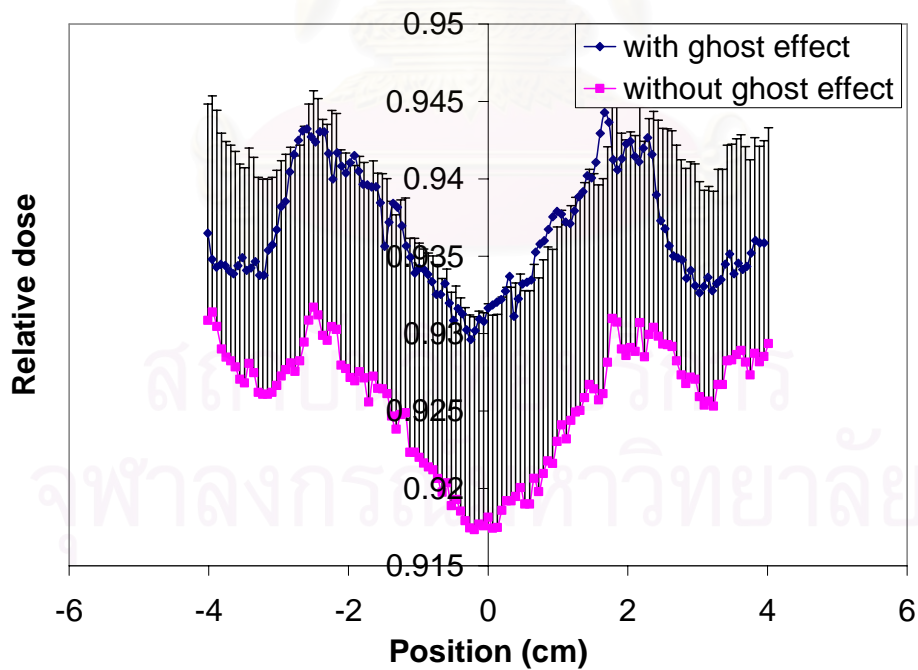

Figure 6.16 The zoom profile in the area of 4 x 4 cm^2

If we adjust the contrast value of the image, we would be able to see clear Ghost Image. However it was found that there would be less error when there was an increasing in time interval between deliveries. The ghost image effect will not usually appear because to change irradiation from one field to next field, it would take more than 15 seconds.

6.3 EPID Dosimetry

6.3.1 Relative dose measurement for open and wedge fields

The comparison between the profile measured by EPID and ion chamber[5,6] of 4 x 4, 10 x 10 and 15 x 15 cm^2 field size are shown in figure 6.17-6.19, respectively. The same comparison of 45^0 and 60^0 of wedge profile of 4 x 4, 10 x 10 and 15 x 15 cm^2 are shown in figure 6.20-6.25. The profile of small open field which was 4 x 4 cm^2 showed slightly higher dose of EPID in the centre of the beam than ion chamber and the two profiles became agreeable within 3% difference in dose and 3 mm. difference in distance for 10 x 10 and 15 x 15 cm^2 field size. The profile of small wedge fields also showed the agreement in the center part but slightly shift in the penumbra region, the shift distance between EPID and ion chamber was within 3.5 mm. The more error was obtained for larger wedge angle. The EPID profiles of large wedge field were more agreeable with ion chamber profile. This effect was due to the input of largest profile during the commissioning of portal dosimetry mode.
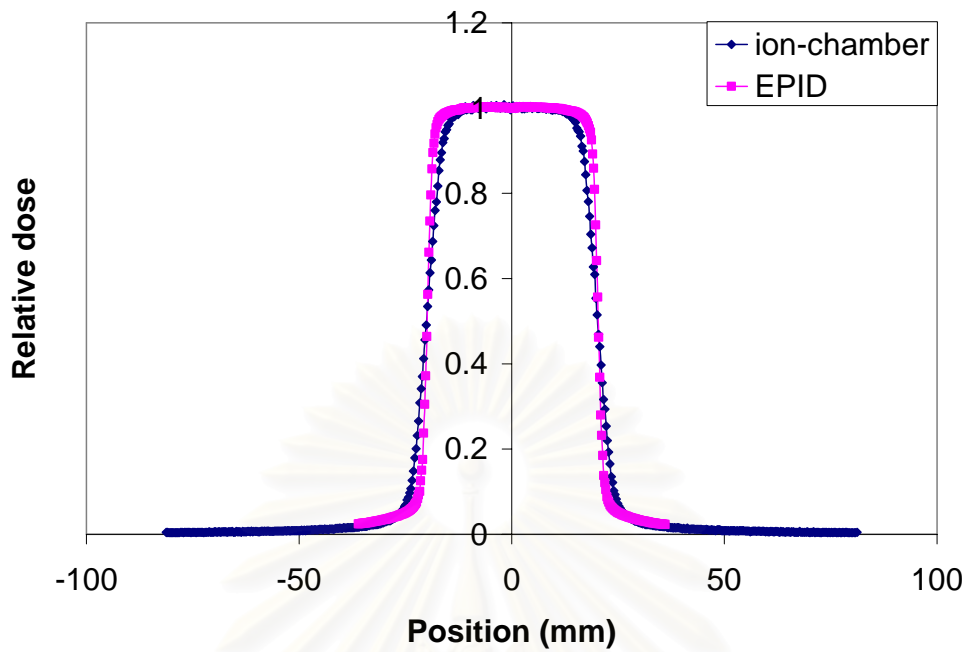
Figure 6.17 The comparison of profiles measured
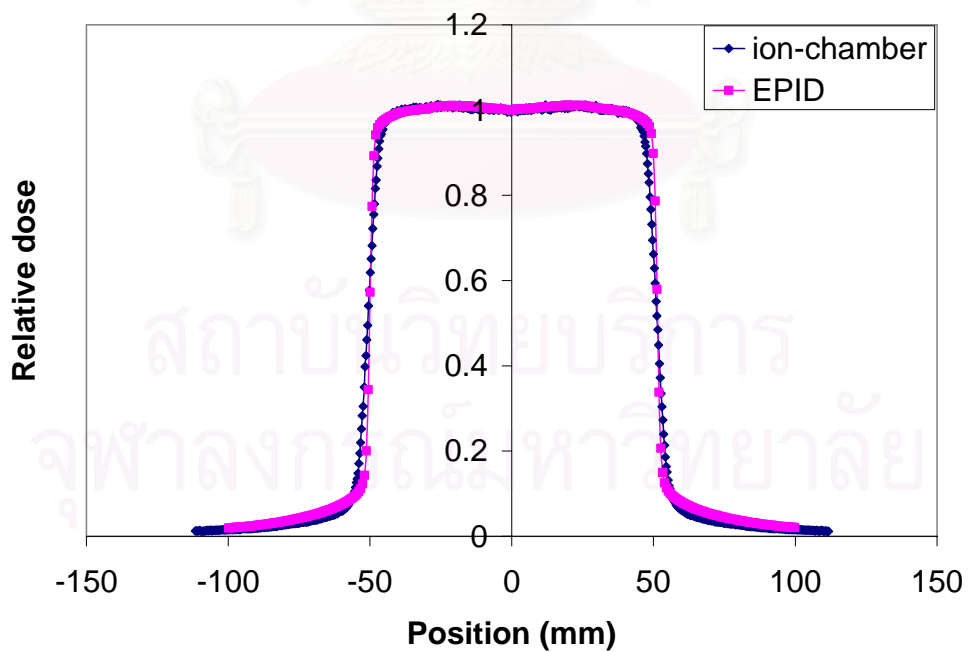by EPID and ion chamber for 4 x 4 cm^2

Figure 6.18 The comparison of profiles measured
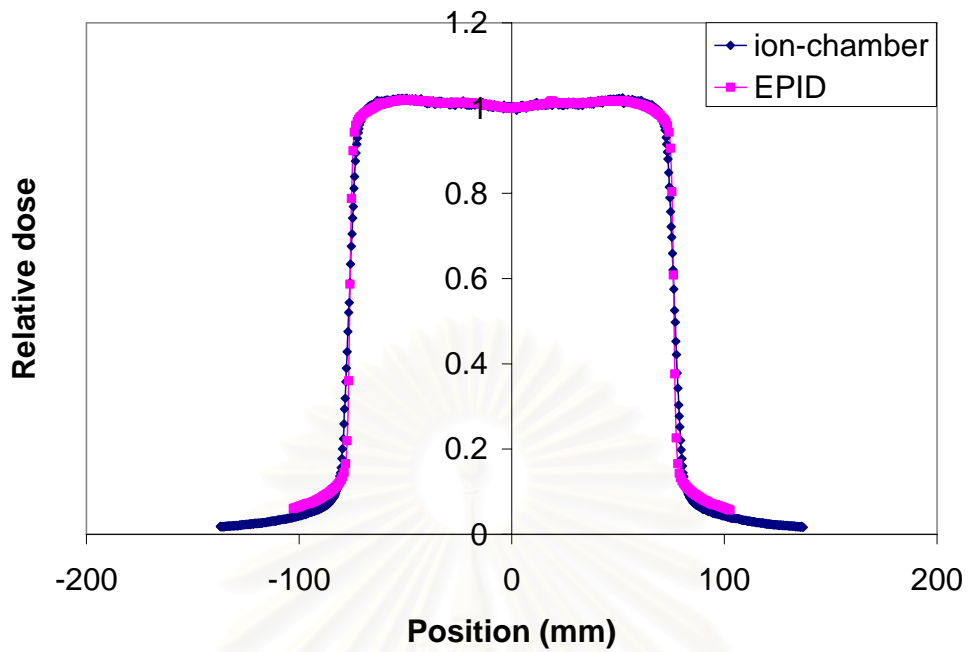by EPID and ion chamber for 10 x 10 cm^2

Figure 6.19 The comparison of profiles measured
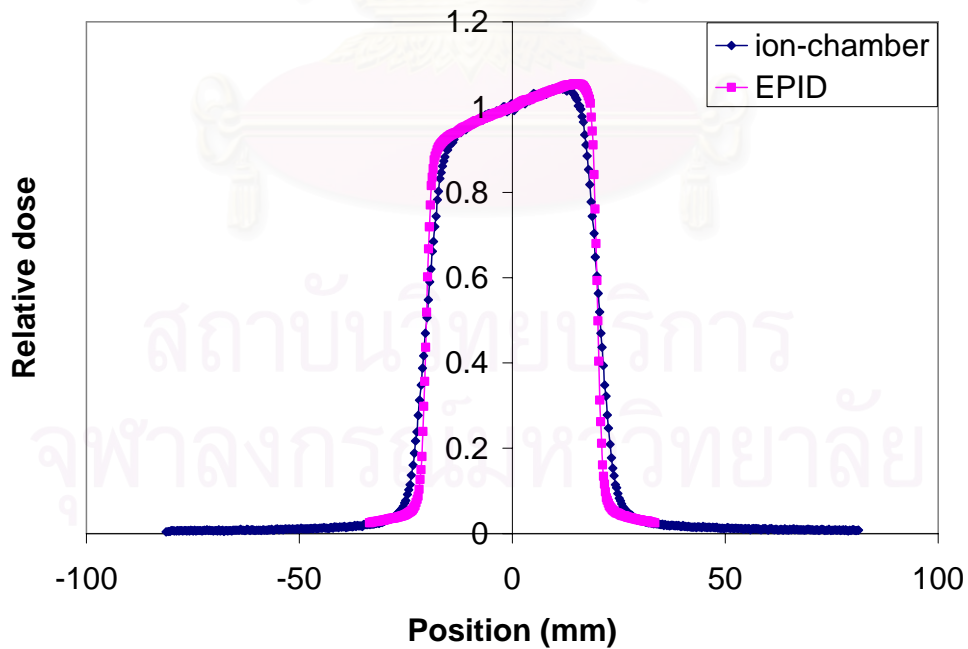by EPID and ion chamber for 15 x 15 cm^2

Figure 6.20 The comparison of profiles measured by EPID
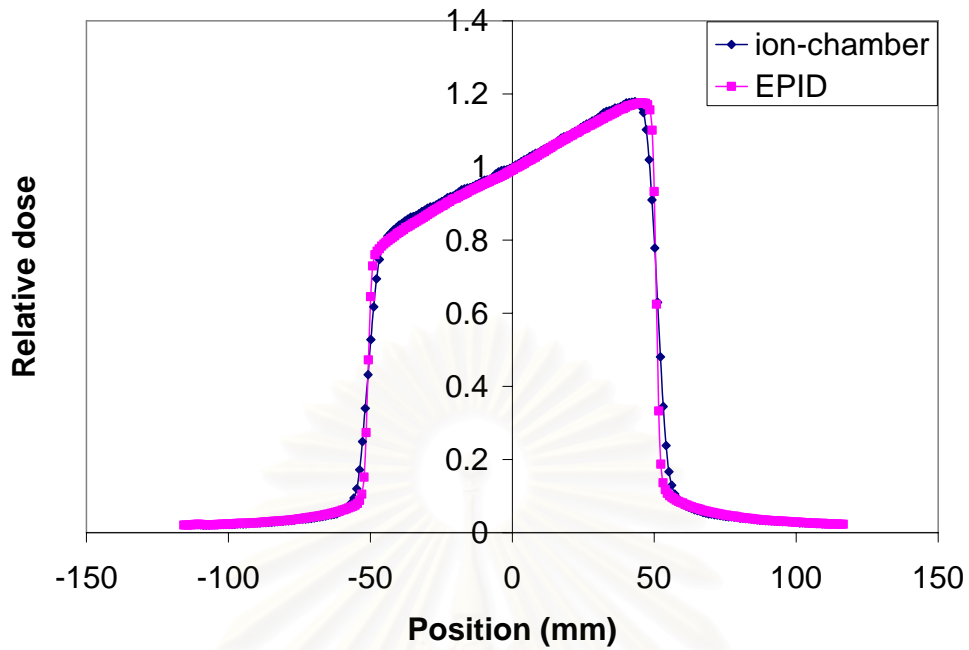and ion chamber for 4 x 4 cm^2 of 45^0 wedge

Figure 6.21 The comparison of profiles measured by EPID
and ion chamber for 10 x 10 cm^2 of 45^0 wedge

Figure 6.22 The comparison of profiles measured by EPID
and ion chamber for 15 x 15 cm^2 of 45^0 wedge

Figure 6.23 The comparison of profiles measured by EPID
and ion chamber for 4 x 4 cm^2 of 60^0 wedge
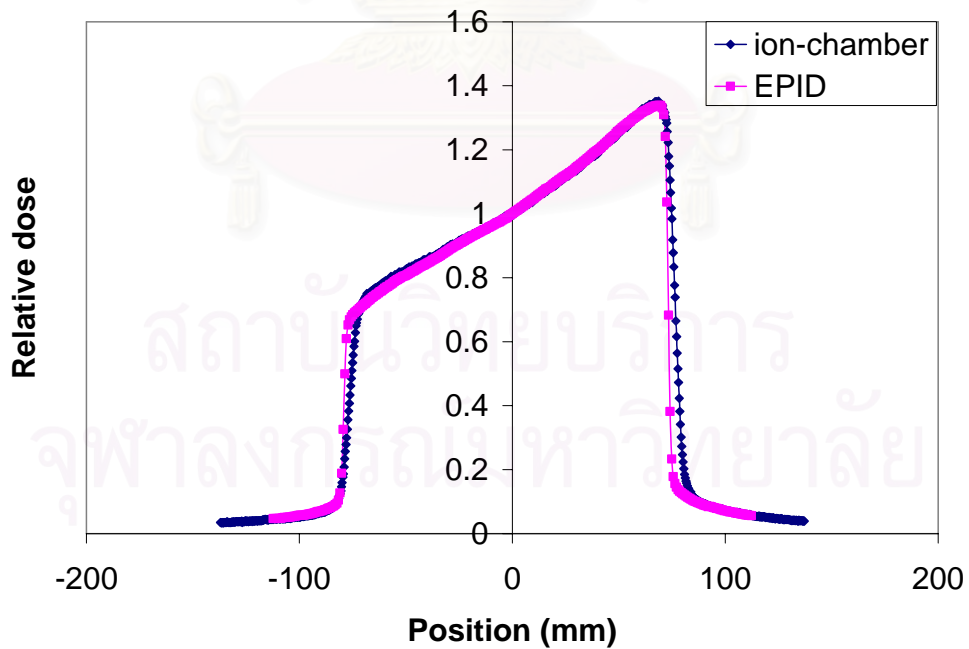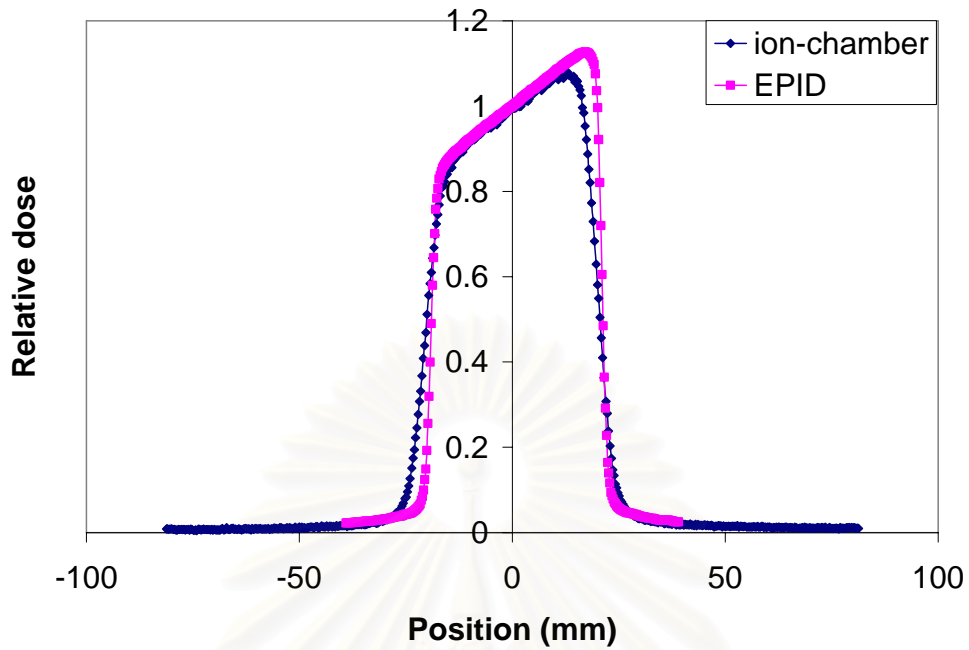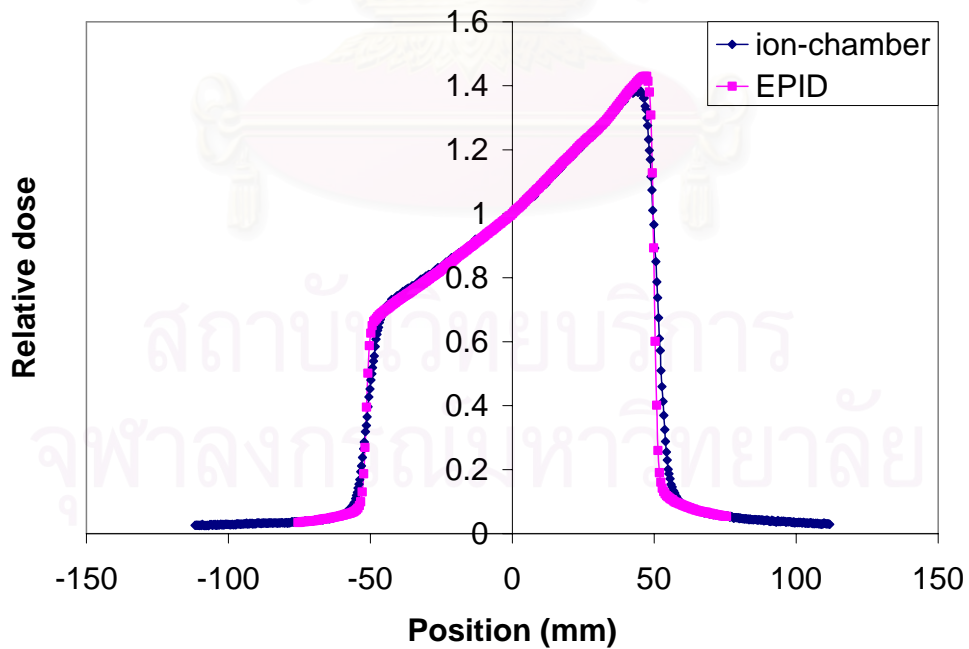

Figure 6.24 The comparison of profiles measured by EPID
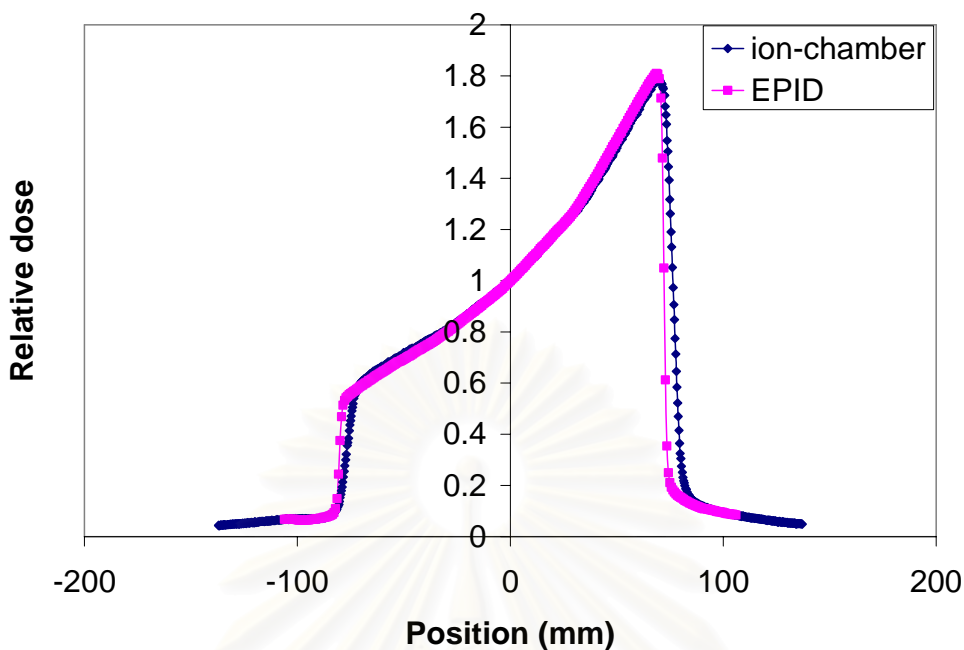and ion chamber for 10 x 10 cm^2 of 60^0 wedge

Figure 6.25 The comparison of profiles measured by EPID
and ion chamber for 15 x 15 cm^2 of 60^0 wedge

6.3.2 IMRT pre-treatment verification

The comparison between EPID calculation and EPID measurement in IMRT
pre-treatment QA[6] of 2 CA-nasopharynx fields are shown in fig 6.26-6.29. The
absolute isodose distribution in fig 6.26 and fig 6.28 show the agreement of
calculation and measurement. The profiles in the direction of MLC in fig 6.27 and fig
6.29 show the agreeable between EPID calculation and EPID measurement within 3%
difference in dose and 3 mm. difference in distance.

———— EPID calculation
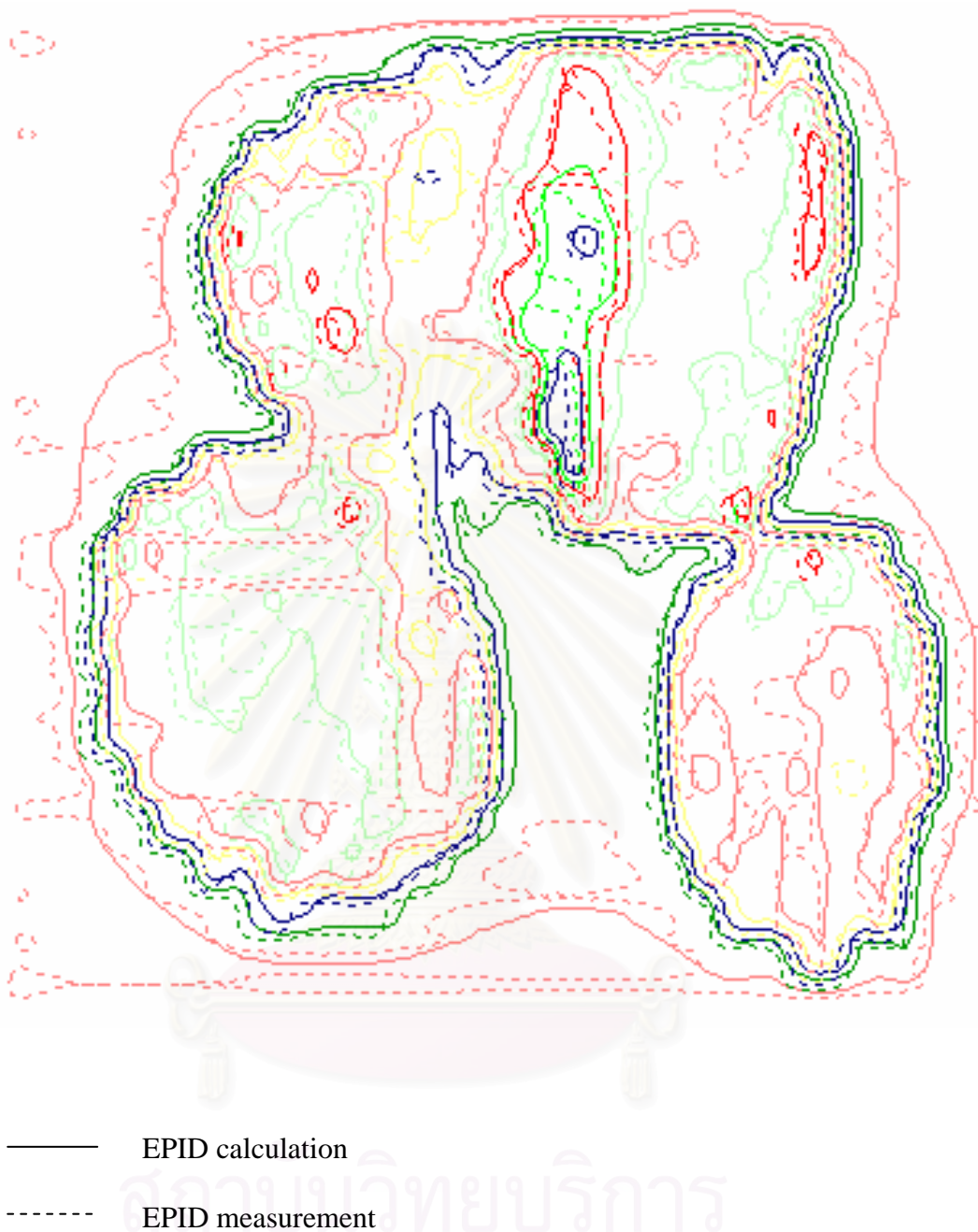
- - - - - - EPID measurement

Dose difference criterion (%) 3
DTA criterion   3
Maximum gamma   2.965031
Average gamma   0.164247
Score   0.994819

Figure 6.26 The comparison of isodose distribution of nasopharynx field 1 between
EPID calculation and EPID measurement

Figure 6.27 The EPID profile in x direction in a plane
as shown in figure 6.26

EPID calculation

------- EPID measurement

Dose difference criterion (%) 3
DTA criterion   3
Maximum gamma   3.266547
Average gamma   0.197165
Score   0.993659

Figure 6.28 The comparison of isodose distribution of nasopharynx field 2 between
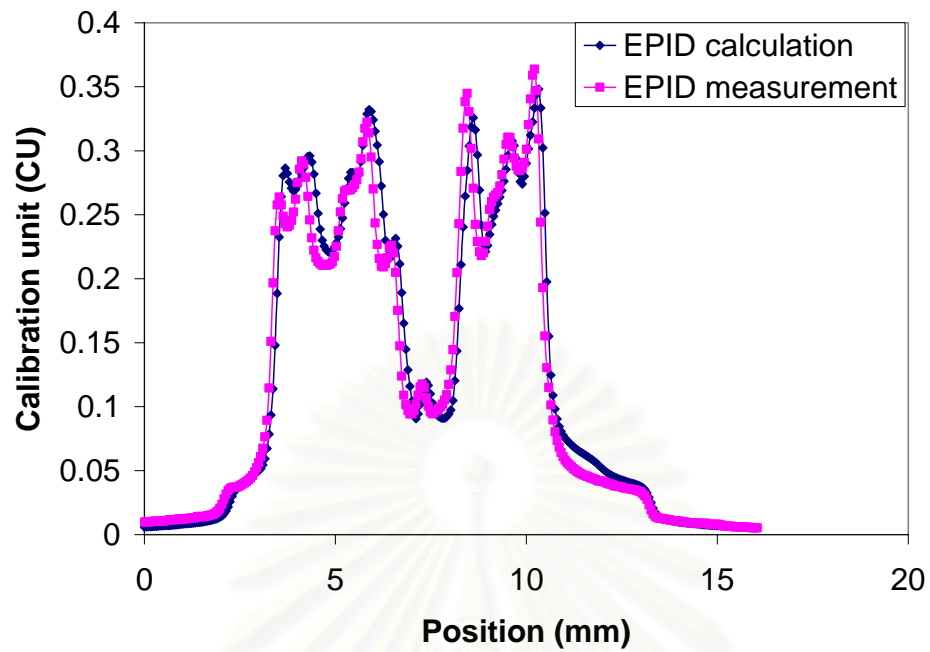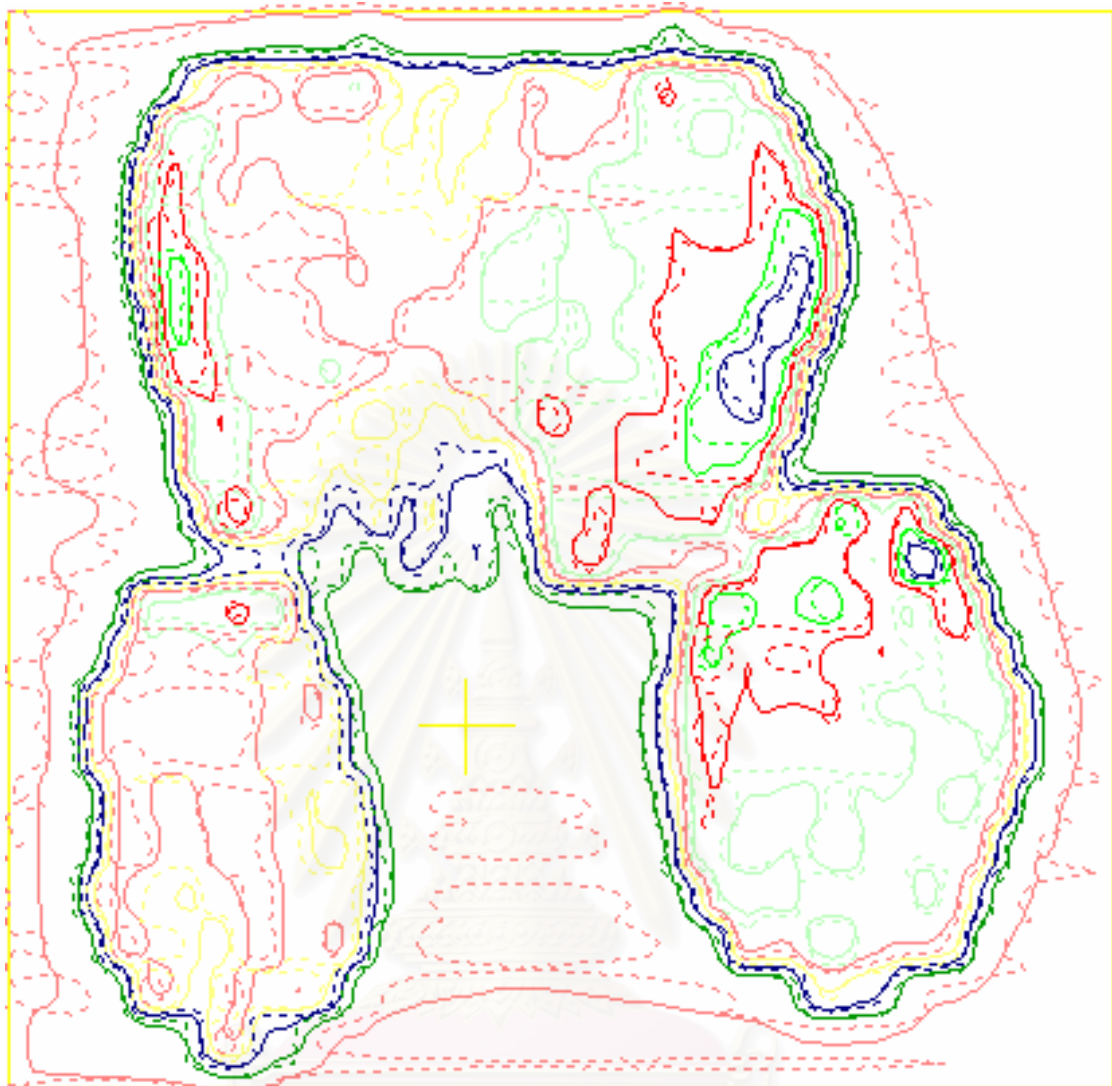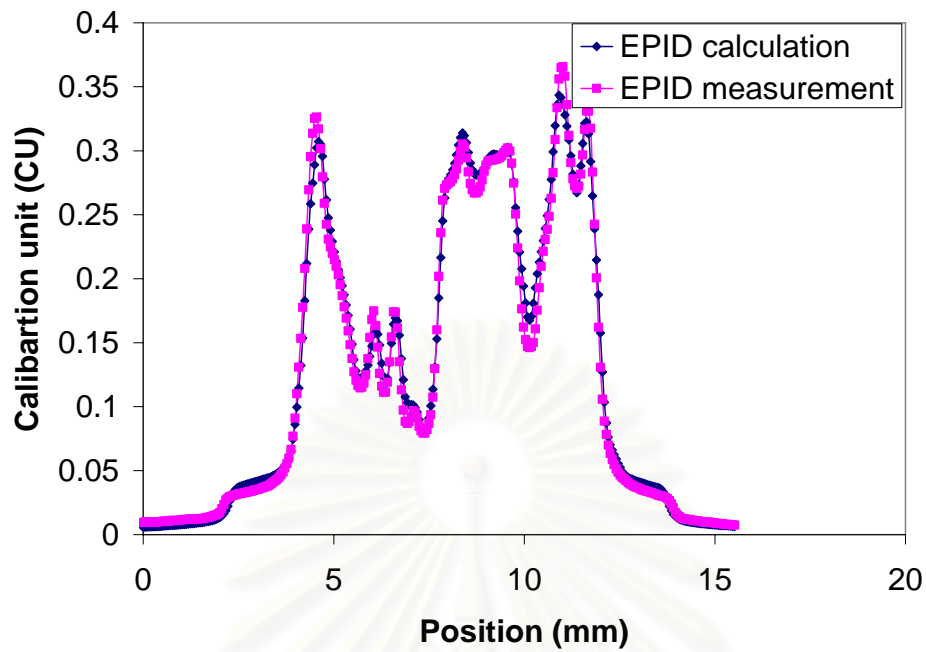EPID calculation and EPID measurement

Figure 6.29 The EPID profile in x direction in a plane
as shown in figure 6.28

CHAPTER VII

CONCLUSIONS

Electronic portal imaging device (EPID) was developed for the purpose of patient setup verification. In addition the dosimetric properties have been extensively studied. More recently the application of flat panel amorphous silicon based EPID to verify dynamic IMRT has been addressed. In this study, the dosimetric properties of amorphous EPIDs was investigated in imaging mode and their application for dynamic IMRT verification was carried on in portal dosimetry mode.

The calibration needed to be performed for accurate response. For using in imaging mode, the image was acquired to correct for non-uniformity in the EPID response, and ideally the beam profile for the FF acquisition should be uniform. The mode for acquired image should be continuous mode for dosimetry to prevent loss signal due to irradiation. The result of dosimetric properties showed that the response of EPID in larger field size was more sensitive than ion-chamber but less in smaller field size, the field studied was 4 x 4 to 24 x 24 cm^2. The EPID showed increasing of signal with the field size more pronounced than ion chamber. The response of EPID was linearity with dose rate and integral dose. The response of EPID in terms of pixel value was not linear with the integral dose, the response variation with integral dose was influenced by the fluctuation of beam dose rate. The dose rate of startup beam was increasing until it was stable, sometimes it fluctuated during irradiation, this made the non-linearity between pixel value and dose. However, the frame would be compensated so the EPID response in terms of pixel value multiplied by number of frames showed linearity with integral dose.

The effect of dead time due to the transfer data to the CPU was found every 64 frames. For static field, the effect of dead time started at 40 MU making less number of frames. So the multiplication of EPID signal with number of frames that considered dead time and non dead time gave the difference values. Considering this different values as the error due to dead time, they increased when the dose was increasing, the field size seemed to be no effect. The maximum error for 10-200 MU and 4 x 4 to 15 x 15 cm^2 field sizes were within 3.60%. For dynamic field, the effect of dead time was studied by sliding window delivery with a uniform 1 cm leaf gap at 0.25-1.0 cm/s. The error increased when the leaf speed was increasing. The maximum error was 17.62% for a leaf speed of 1.0 cm/s. There was no effect of dose rate fluctuation in dynamic field for EPID readout. This result agrees with Greer and Popescu[5] who showed that the EPID can accurately record the rapid dose rate changes that occur with leaf speeds up to 2.5 cm/s. The memory effect was found negligible when time interval between two deliveries was more than 15 sec.

When using the EPID portal dosimetry mode, the profiles for static field of 4 x 4, 10 x 10 and 15 x 15 cm^2 from EPID and ion chamber measurement were compared. They were agreeable well, only small field of 4 x 4 cm^2 showed slightly higher dose of EPID in the centre of the beam. For wedge field, both of EPID and ion chamber profiles showed the agreement in the center part but slightly shift in the penumbra region. The shift distance was within 3.5 mm. The larger wedge angle gave more shift than smaller wedge angle.

An important dosimetric application of portal dosimetry is the verification of IMRT treatment plans. The performance of the amorphous silicon detector was assessed for pre-treatment dosimetric measurement of IMRT beam delivery.
The pre-treatment verification of cancer of nasopharynx IMRT planning was demonstrated to determine the ability of using EPID as a dosimeter. The example of two fields in nasopharynx plan showed the agreeable of absolute dose distribution between EPID calculation and EPID measurement within 3% difference in dose and 3 mm. difference in distance. The profile in the direction of MLC movement showed good correlation between calculation and measurement.

The EPID proves to be a convenient and accurate detector for static as well as dynamic portal dosimetry, when operated in the portal dosimetry mode. Although the behavior of the EPID measurement is not equivalent to a dose to water measurement, it is self-consistent and reproducible. Hence, an absolute portal dose image prediction could be developed allowing verification of the actual fluence delivery of individual IMRT fields. Portal dosimetry provides a tool for routine, pre-treatment QA of IMRT treatments that is potentially significantly faster and more convenient than current pre-treatment methods.

However, the limiting of EPID used as a dosimeter is the degradation of sensitivity, so EPID need to be recalibration every month. The other limiting is the EPID can be used in pre-treatment of IMRT only in a single gantry angle, each radiation beam is aimed independently at the dosimeter beam in the vertical direction. Thus, validation is conducted on a beam by beam basis and the doses are compared independently for each beam. The composite beam of all fields treated could not be done.This work has been undertaken only for single photon beam of 6 MV and single beam pulse of 300 MU/min. Further study of other photon energy at different beam pulse needs to design so that the characteristic of the beam could be determined and be used accurately. The sensitivity of EPID needs to be observed for longer period time. Recently, EPID which allowed in-phantom dosimetry was developed[3], this option has not yet been widely available in commercial treatment planning systems. This program would make it be easier to calculate dose using treatment planning software without buying the extra software. This requires the development of the in-house algorithm to predict the portal dose. So the development of portal dosimetry is still going on in our department.

REFERENCES

1. Van, E. A., et al. 2002. Acceptance tests and quality and control procedures for the clinical implementation of intensity modulated radiotherapy (IMRT) using inverse planning and sliding windows technique. Radiother Oncol 65: 53-70.

2. Antonuk, L. E., et al. 1992. Demonstration of megavoltage and diagnostic x-ray imaging with hydrogenated amorphous silicon arrays. Med Phys 19: 1455-1466.

3. Moran, J., et al. 2005. An active matrix flat panel dosimeter (AMFPD) for in-phantom dosimetric measurements. Med Phys 32: 466-472.

4. Van, E. A., et al. 2001. Pre-treatment dosimetric verification by mean of a liquid-filled electronic portl imaging device during dynamic devery of intensity modulated treatment fields. Radiother Oncol 60: 181-190.

5. Greer, P., and Popescu C. 2003. Dosimetric properties of an amorphous silicon electronic portal imaging device for verification of dynamic intensity modulated radiation therapy. Med Phys 30: 1618-1627.

6. Van, E. A., et al. 2004. The use of an aSi-based EPID for routine absolute dosimetric pre-treament verification of dynamic IMRT fields. Radiother Oncol 71: 223-234.

7. McCurdy, B., and Pistorius S. 2000. A two-step algorithm for predicting portal dose images in arbitrary detectors. Med Phys 27: 2109-2116.

8. McCurdy, B., and Pistorius S. 2001. Dosimetric investigation and portal dose image prediction using an amorphous silicon electronic portal imaging device. Med Phys 28: 911-924.

9. Winkler, P., et al. 2005. Dose-response characteristic of an amorphous silicon EPID. Med Phys 32: 3095-3105.

10. Samual, H. 2003. A practical guide to intensity-modulated radiation therapy. Madison: Memorial Sloan-Kettering Cancer.

11. Williams, P. C. 2003. IMRT:delivery techniques and quality assurance. BJR 76: 766-776.

12. Langmack, K. A. 2001. Portal imaging. BJR 74: 789-804.

13. Jerrold, T. B., et al. 2002. The essential physics of medical imaging. Philadelphia: Wolter Kluwer.

14. Vetteli, D., et al. 2004. Introduction of a novel dose saving acquisition mode for the PortalVisionTM aS500 EPID to facilitate on-line patient setup verification. Med Phys 31: 828-831

15. Heinrich, R. 2002. Varian Medical Systems. Switzerland: Baden.

16. Storchi, L., et al. 1996. Calculation of the absorbed does distribution due to irregularly shaped photon beam using pencil beam kernels derived from basics data input. Phys Med Biol 41: 637-657.

APPENDIX

Image Orientation

The image orientation on the PortalVision screen related to the treatment unit is shown in the figure below. The image consists of 512 x 384 pixels.
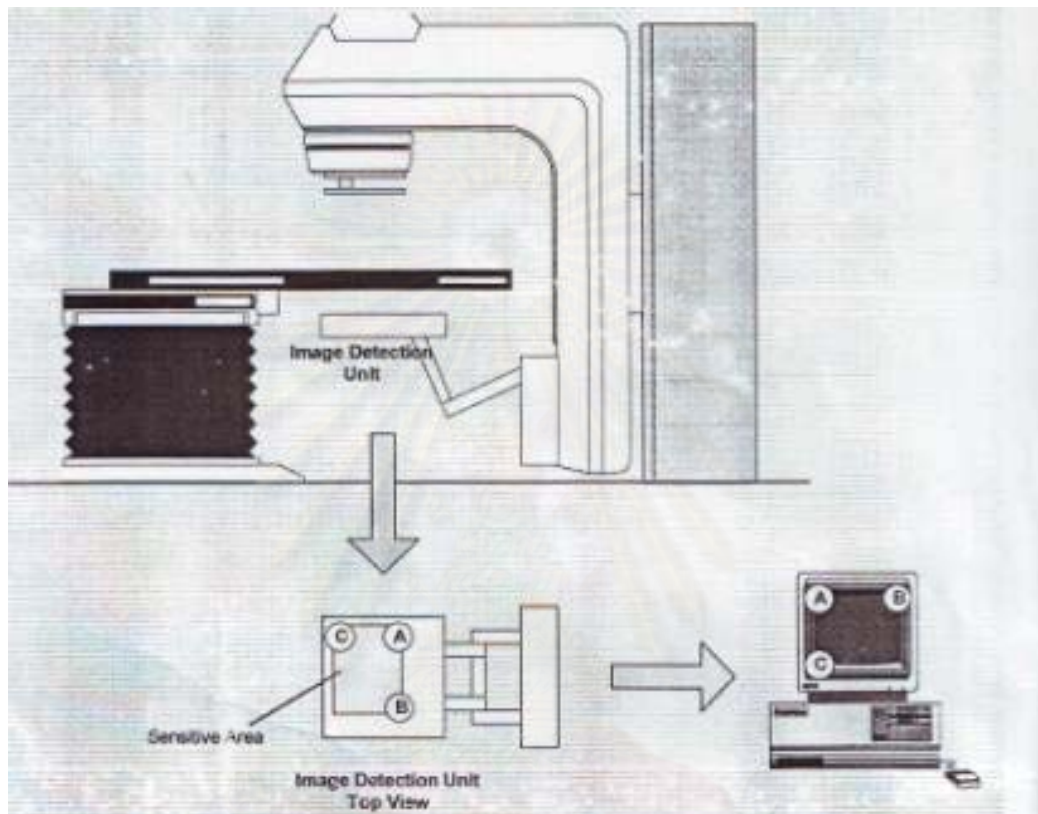

Figure 9.30 Image orientation

Image coordinates according to fig 9.30 above

Coordinate	Row	Column
A	1	1
B	1	512
C	384	1

VITAE

NAME	Mr. Nuttakorn Preedasak
SEX	Male
NATIONALITY	Thai
DATE OF BIRTH	9 August 1982
PLACE OF BIRTH	Bangkok, Thailand
INSTITUTIONS ATTENDED	Chulalongkorn University, 2000: Bachelor of Science (Physics)
	Chulalongkorn University, 2004: Master of Science (Medical Imaging)
HOME ADDRESS	90/1 Soi. Pramsombat 3 Prachasongkror Road Dindang Bangkok 10400 Thailand Tel. 02-274-6202